

Multiple fault reactivations within the intra-continental Rhine–Bresse Transfer Zone (La Serre Horst, eastern France)

Herfried Madritsch^{a,*}, Alexandre Kounov^{a,1}, Stefan M. Schmid^{a,2}, Olivier Fabbri^{b,3}

^a Geologisch-Paläontologisches Institut, Universität Basel, Bernoullistr. 32, CH-4056 Basel Switzerland

^b UMR 6294 Chrono-Environnement, Université de Franche-Comté, Route de Gray 16, F-25030 Besançon cedex, France

ARTICLE INFO

Article history:

Received 16 June 2008

Received in revised form 6 February 2009

Accepted 27 February 2009

Available online 11 March 2009

Keywords:

Fault reactivation

Fission-track dating

Paleostress analysis

La Serre Horst

Rhine–Bresse Transfer Zone

France

ABSTRACT

Thermochronological, structural and kinematic analyses demonstrate the influence of Late Paleozoic basement structures on the localization and evolution of the Rhine–Bresse Transfer Zone (RBTZ), a central segment of the European Cenozoic Rift System. Zircon and apatite fission track data indicate that the Paleozoic crystalline basement and its Permo-Triassic cover, exposed in the La Serre Horst, experienced a Middle Jurassic to Early Cretaceous heating event which was followed by two distinct periods of cooling. A first cooling event occurred in the Early Cretaceous and is probably related to thermal relaxation. A second one, started at around 38 Ma, is interpreted to reflect exhumation that was induced by fault reactivation along the Late Paleozoic Burgundy Trough System during Eocene–Oligocene rifting and the formation of the RBTZ. This fault reactivation resulted in a complex fault pattern and local stress field perturbations in the surroundings of the pre-existing horst structure. Substantial extension was achieved by ENE–WSW striking normal faults that trend highly oblique to the dominant strike of the Rhine and Bresse Graben rifts. Seismic reflection data show that these major normal faults are typically associated with extensional flexures and oriented parallel to pre-existing Late Paleozoic basement faults of the Burgundy Trough. Paleostress analyses yield overall NW–SE extension during the Eo-Oligocene, slightly oblique to the structural trend of the RBTZ, and additionally, local stress field perturbations induced by the reactivation of pre-existing faults. Reactivation of Paleozoic structures in the RBTZ is of extensional rather than of strike-slip character indicating that the RBTZ is forming a separate oblique graben segment within the European Cenozoic Rift System rather than a sinistral strike slip transform zone supposedly connecting Rhine and Bresse graben structures.

© 2009 Elsevier B.V. All rights reserved.

1. Introduction and objectives

The influence of Paleozoic basement discontinuities on the Cenozoic structural evolution of the northwestern Alpine foreland, particularly the formation and evolution of the European Cenozoic Rift System, has been widely discussed by numerous authors (Laubscher, 1970; Illies, 1981; Ziegler, 1992; Lacombe et al., 1993; Schumacher, 2002; Dèzes et al., 2004; Michon and Sokoutis, 2005). This contribution addresses the evolution of the intra-continental Rhine–Bresse Transfer Zone (RBTZ), also referred to as the Rhine–Sàone Transform Zone (Bergerat and Chorowicz, 1981), which forms a central segment

of the European Cenozoic Rift System. Several authors proposed that Eo-Oligocene crustal extension, responsible for the opening of the Rhine and Bresse Graben, was transferred along the RBTZ by sinistrally transpressive reactivation of an ENE–WSW striking Paleozoic basement fault system (e.g. Laubscher, 1970; Illies, 1972; Contini and Theobald, 1974; Bergerat, 1977; Bergerat and Chorowicz, 1981; Lacombe et al., 1993). This concept was based on map interpretation and kinematic studies on brittle deformation of the Mesozoic cover, but also inspired by analogue and numerical modelling (Elmohandes, 1981; Lacombe et al., 1993; Ustaszewski et al., 2005b). However, direct field evidences in favour of reactivation of Paleozoic basement structures during the Eocene–Oligocene formation of the RBTZ are still scarce. Moreover, the subsurface structures within the Paleozoic basement underlying the area of the RBTZ are poorly known. Hence, the previously proposed models regarding transfer zone formation by structural inheritance appear very simplified in view of the complex fault geometries.

This study aims to fill some of these gaps by combining fission track data with extensive structural and subsurface analyses. The latter are based on seismic reflection data that became available to academic institutions for the first time.

The investigation focuses on the La Serre Horst (LSH) which is located in the western part of the RBTZ. This is the only place between

* Corresponding author. Now at: Nagra, Hardstrasse 73, CH-5430 Wettingen, Switzerland. Tel.: +41 56 43 71 249.

E-mail addresses: herfried.madritsch@nagra.ch (H. Madritsch), a.kounov@unibas.ch (A. Kounov), schmid@zedat.fu-berlin.de (S.M. Schmid), olivier.fabbri@univ-fcomte.fr (O. Fabbri).

¹ Tel.: +41 61 267 36 10; fax: +41 61 2673613.

² Now at: Institut für Geologische Wissenschaften, Freie Universität Berlin, Malteserstrasse 74b-100, D-12249 Berlin, Germany. Tel.: +49 30 838 70288; fax: +49 30 838 70734.

³ Tel.: +33 3 81 66 62 75; fax: +33 3 81 66 65 58.

the French Massif Central and the Vosges Mountains basement complexes (Fig. 1) where Paleozoic granites and overlying Permian deposits crop out. Similarly to these much larger basement complexes, the LSH forms a topographic high today. Our combined dataset allows constraining the exhumation history of this horst in order to clarify its influence on fault geometries and kinematics of the Cenozoic RBTZ.

2. Geological setting

The roughly N–S striking European Cenozoic Rift System (ECRIS) dissects Western Europe from the North Sea to the Mediterranean over a distance of about 1100 km (e.g. Dèzes et al., 2004; inset Fig. 1). The northern part of the rift system consists of the Upper and Lower Rhine Graben (URG and LRG respectively) and the Eger Graben in the Bohemian Massif (Ziegler, 1992). The southern part comprises the Bresse Graben (BG), the grabens within the Massif Central (MC), such as the Limagne Graben (LMG) (Merle et al., 1998; Michon and Merle, 2001) and the grabens of the Lower Rhone Valley (Séranne, 1999). The URG, and the BG, representing central segments of this rift system, are connected by the approximately 200 km long ENE–WSW striking intra-continental RBTZ. The northern part of the RBTZ cuts through the autochthonous Mesozoic sediments of the Burgundy Platform and is flanked to the northeast by the basement of the Vosges Mountains.

To the south, the RBTZ is bordered, and partially overridden, by the thin-skinned Neogene Jura fold-and-thrust belt (Fig. 1, Chauve et al., 1980; Madritsch et al., 2008).

The sedimentary record of the southern URG constrains the opening of the ECRIS between Middle (42.5 Ma, Lutetian; Berger et al., 2005; Hinsken et al., 2007) to Late Eocene times (36 Ma, Late Priabonian, Sissingh, 1998). Mechanisms controlling the opening and the following evolution of the ECRIS have been debated for a long time and the proposed models range from hot-spot driven active rifting (Neugebauer, 1978) to passive rifting model, the latter being possibly induced by collisional foreland splitting (Sengör, 1976; Dèzes et al., 2004), back-arc extension (Jowett, 1991) or slab-pull (Merle and Michon, 2001). Many authors suggested that during the main stage of rifting in the Eocene–Oligocene, the RBTZ transferred crustal extension from the Rhine to the Bresse Graben (Laubscher, 1970; Illies, 1972; Contini and Theobald, 1974; Bergerat and Chorowicz, 1981) whereby different kinematic models were evoked (e.g. Bergerat, 1977; Lacombe et al., 1993).

The southern URG as well as the RBTZ were affected by large-scale differential uplift after the main phase of rifting. This uplift probably started in Early Miocene time (Aquitainian; Berger et al., 2005) but is so far well constrained only for the Middle Miocene (Burdigalian; Schumacher, 2002; Ziegler and Dèzes, 2007). From the Early to Middle

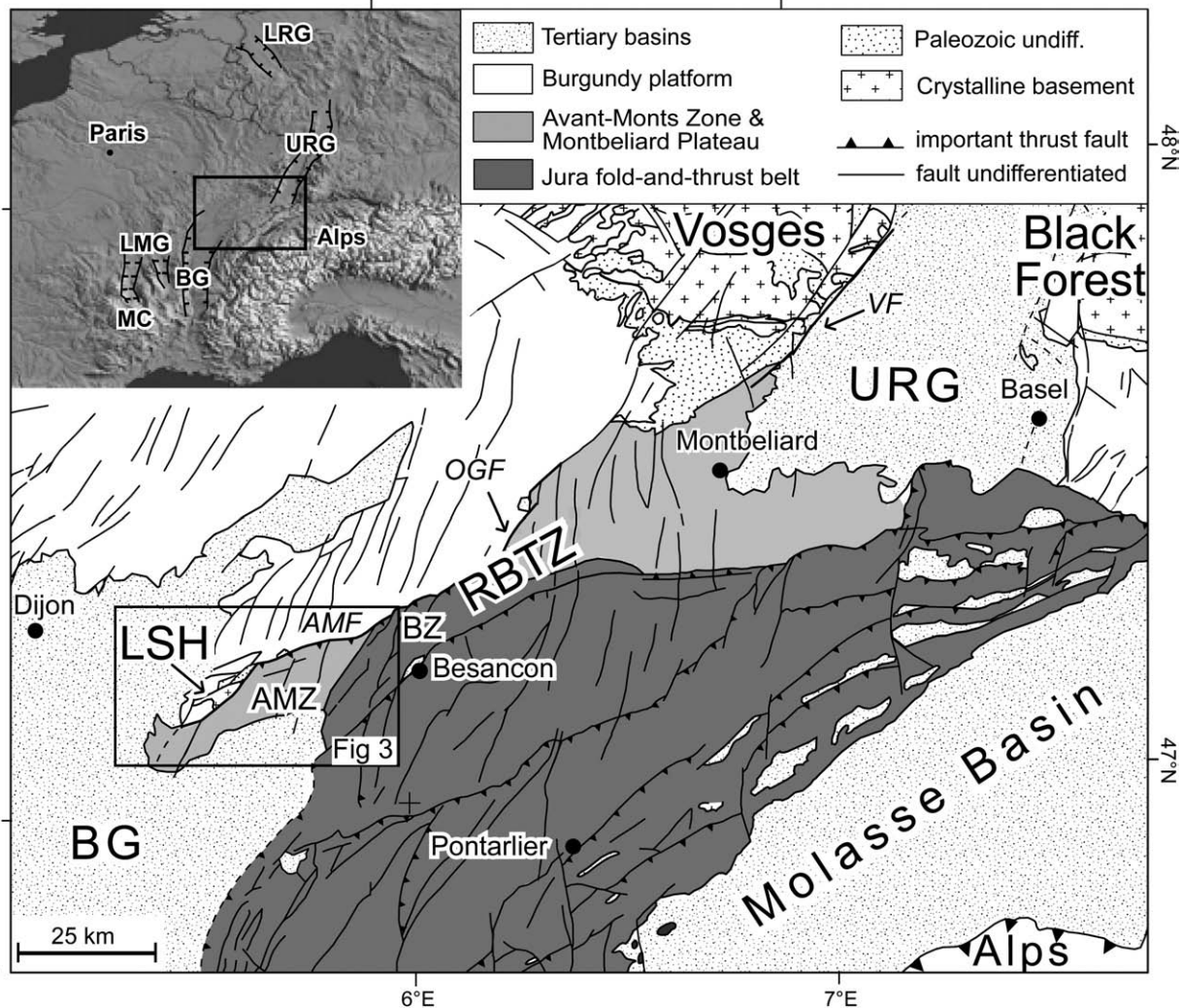


Fig. 1. Geological setting of the study area. The Rhine–Bresse Transfer Zone (RBTZ) is a segment of the European Cenozoic Rift system (inset) located between the Rhine and Bresse grabens. The La Serre Horst (LSH) forms an isolated crystalline massif at the western termination of the RBTZ. The tectonic units are drawn as defined in Madritsch et al. (2008). AMF: Avant-Monts Fault; AMZ: Avant-Monts Zone; BG: Bresse Graben; BZ: Besançon Zone; MC: Massif Central; LMG: Limagne Graben; LRG: Lower Rhine Graben; LSH: La Serre Horst; OGF: Ognon Fault; RBTZ: Rhine–Bresse Transfer Zone; URG: Upper Rhine Graben; VF: Vosges Fault.

Miocene the axis of this uplift apparently shifted NW-ward (Schumacher, 2002; Rocher et al., 2003). This has been variably interpreted as reflecting the outward migration of the Alpine flexural fore-bulge (Laubscher, 1992; Schumacher, 2002) or as the effect of collision-related compressional deformation involving lithospheric folding (Dèzes et al., 2004; Bourgeois et al., 2007; Ziegler and Dèzes, 2007). As a consequence of this uplift and erosion the Oligocene rift related sediments, testimony of former rift-related depocenters (Chauve et al., 1983; Dreyfuss and Kuntz, 1969; Fig. 1), are only locally preserved within the RBTZ area.

From the Late Miocene, crustal shortening and nappe stacking in the external crystalline massifs of the Central Alps induced the formation of the thin-skinned Jura fold-and-thrust belt (Laubscher 1972; Burkhard, 1990; Schmid et al., 1996). By the Early Pliocene its northwestern-most segment, the Besançon Zone (Fig. 1), encroached onto the RBTZ (Madritsch et al., 2008). Further stress build-up in response to ongoing Alpine collision caused subsequent thick-skinned reactivation of the RBTZ at the north-western margin of the Jura fold-and-thrust belt. This is associated with partial inversion of pre-existing Paleozoic and Paleogene basement rooted normal faults. Such inversion during compressional to dextral transpressive deformation is well documented from seismic reflection data throughout the Avant-Monts Zone (Madritsch et al., 2008; Fig. 1). It is also reported from the easternmost part of the RBTZ (Giamboni et al., 2004; Rotstein et al., 2005b; Ustaszewski and Schmid, 2007) and from within the Jura Mountains (Roure, 2008). Present day low to medium seismicity of the area suggests that thick-skinned tectonics are still ongoing (Ustaszewski and Schmid, 2007; Madritsch et al., 2008).

According to many authors the RBTZ formed during Eocene–Oligocene by structural inheritance and reactivation of the Late Paleozoic Burgundy Trough (e.g. Laubscher, 1970; Illies, 1972; Ziegler, 1992; Schumacher, 2002; Ustaszewski et al., 2005a; Fig. 2). This roughly ENE–WSW striking Permo–Carboniferous graben system extends over a distance of about 300 km from the northern parts of the Massif Central through the Bresse Graben into the area of the RBTZ and further to Basel where it links with the Permo–Carboniferous graben system of Northern Switzerland and Southern Germany (Boigk and Schönreich, 1970; Debrand-Passard and Courbouleix, 1984; Bergerat et al., 1990; Diebold and Naef, 1990; Ziegler et al., 2004).

The northern and southern boundaries of the Burgundy Trough System are poorly constrained. Most authors report an approximate width of about 50 km (e.g. Debrand-Passard and Courbouleix, 1984; Ziegler et al., 2004; Fig. 2). Deep well logs in the central part of the transfer zone document graben depths of over 800 m and indicate that graben formation started in Late Carboniferous times (Chauve et al., 1983). The formation of the Burgundy Trough was probably related to the activity along a dextral transpressive trans-European shear zone and was accompanied by volcanism (Ziegler, 1986; Schumacher, 2002; McCann et al., 2006).

The NE–SW striking La Serre Horst (LSH, Figs. 1–3) is part of a larger basement high within the Burgundy Trough, referred to as the La Serre Horst Structure (LSHS in Fig. 2). This basement high is located at the transition between the northern Bresse Graben and the RBTZ. To the southwest the La Serre Horst Structure connects with the Sennecey High of the northern central Bresse Graben (e.g. Rat, 1976; Bergerat et al., 1990; Rocher et al., 2003). The LSH is part of the Paleozoic La Serre Horst Structure and is the only place where Paleozoic rocks are presently exposed at the surface (Morre and Thiébaud, 1961; Chauve et al., 1983; Coromina and Fabbri, 2004; Figs. 1, 3 and 4). In the LSH a ductile to brittle low-angle fault zone separates a Middle Carboniferous granite in the footwall (317 ± 5 Ma, U–Th/Pb monazite EMPA dating, Choulet et al., 2007; Choulet pers. communication) from Permian volcanics and conglomerates in the hanging wall (Coromina and Fabbri, 2004; Fig. 4). In this study the low-angle fault zone (La Serre Median Fault Zone, Coromina & Fabbri, 2004) will be referred to as the La Serre Detachment (Figs. 3 and 4). The fault zone shows a top-to-the-NE sense of shear (Coromina and Fabbri, 2004). The granite, in the detachment's footwall, exhibits a magmatic foliation that grades into a mylonitic foliation near the La Serre Detachment (Coromina and Fabbri, 2004), indicating that the exhumation of the granite and the surrounding metamorphic Variscan basement along the La Serre Detachment occurred during or shortly after granite intrusion. Lower Triassic sandstones (Buntsandstein formation; Coromina and Fabbri, 2004) seal the detachment, which indicates that the activity along this fault terminated in latest Paleozoic times. The northern limit of the LSH is formed by a set of NNW-dipping high-angle brittle normal faults cutting the La Serre Detachment. To the southeast the LSH is bound by the late-stage high-

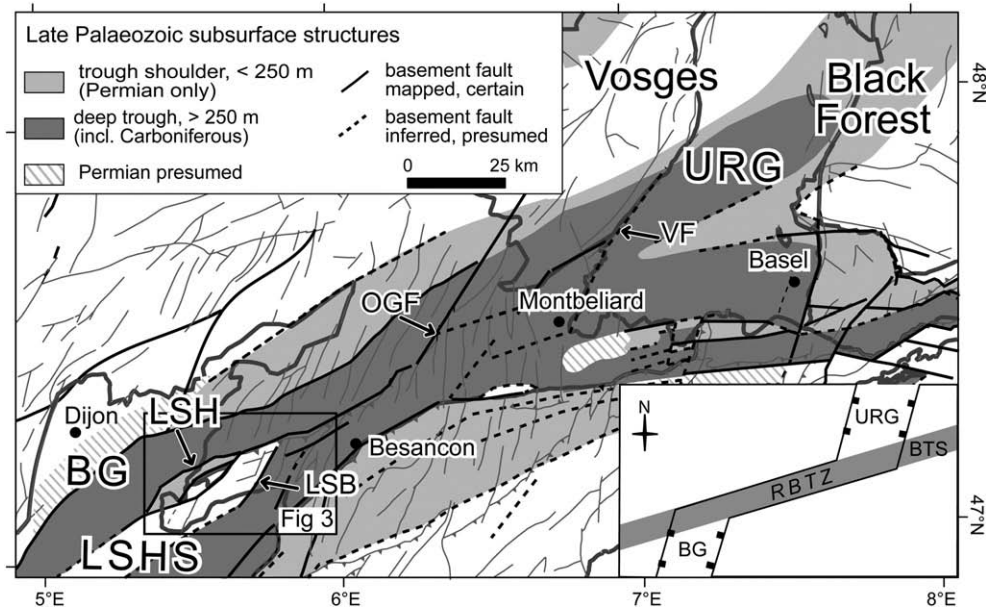


Fig. 2. Subsurface map of the Rhine–Bresse Transfer Zone (RBTZ), modified after Debrand-Passard and Courbouleix (1984) and Ustaszewski et al. (2005a,b). The Eocene–Oligocene RBTZ is oriented parallel to the Late Paleozoic Burgundy Trough System and is believed to have formed due to structural inheritance from this pre-existing fault pattern (see sketch in the lower right). BG: Bresse Graben; BTS: Burgundy Trough System; LSB: La Serre Border Fault; LSH: La Serre Horst; LSHS: La Serre Horst Structure; OGF: Ognon Fault; RBTZ: Rhine–Bresse Transfer Zone; URG: Upper Rhine Graben; VF: Vosges Fault.

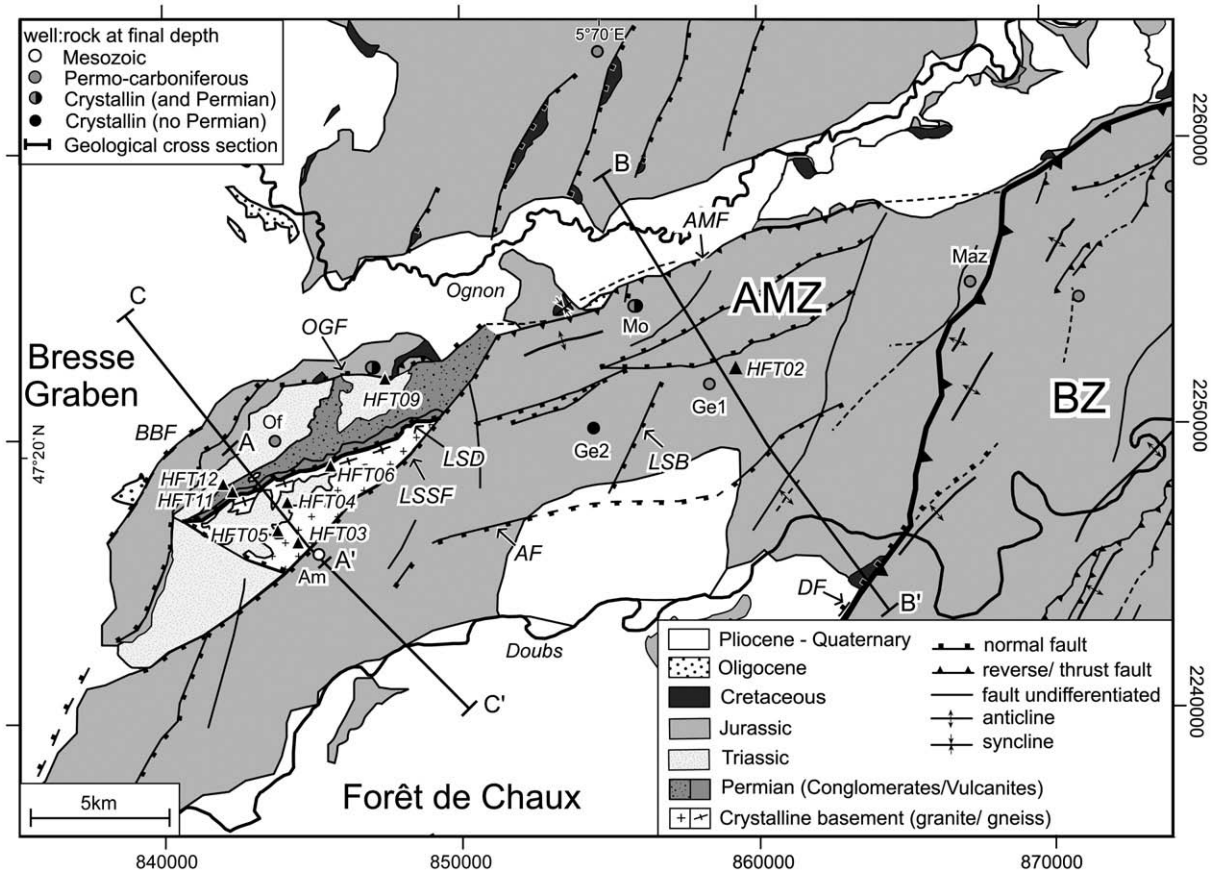


Fig. 3. Geological map of the study area, indicating the location of wells with signatures (Figs. 6, 7 and 14) and the trace of the geological cross sections (Fig. 14). Triangles mark the location of fission track samples from the La Serre Horst and its surroundings (see also Fig. 4 for details). The thick black line marks the front of the Besançon Zone that is part of the thin-skinned Jura fold-and-thrust belt. AF: Arne Fault; AMF: Avant-Monts Fault; AMZ: Avant-Monts Zone; BZ: Besançon Zone; BBF: Bresse Border Fault; DF: Doubs Fault; LSB: La Serre Border Fault; LSD: La Serre Detachment; LSSF: La Serre Southern Fault; OGF: Ognon Fault.

angle La Serre Southern Fault (Coromina and Fabbri, 2004; Figs. 3 and 4) that down faults the part of the La Serre Horst Structure, presently preserved only in the subsurface (Fig. 2).

3. Fission track analysis

3.1. Methodology

The samples for zircon and apatite fission track dating were collected along a NW–SE striking profile across the La Serre Horst (Figs. 3 and 4, Table 1). The samples include Late Paleozoic granites and gneisses, and Permian to Early Triassic volcanics, conglomerates

and sandstones. One sample is a Liassic claystone collected from the Mesozoic cover of the La Serre Horst, about 12 km east of the main traverse (sample HFT02; Fig. 3).

Sample preparation followed the routine technique described in Seward (1989). Etching of the apatite grains used 7% HNO₃ at 21 °C for 50 s. Zircon grains were etched in a eutectic mixture of KOH and NaOH at 220 °C between 9 and 15 h. Irradiation was carried out at the OSU facility, Oregon State University Radiation Center, USA. Microscopic analysis was completed at Basel University using an optical microscope with a Kinetek computer-driven stage (Dumitru, 1995). All ages were determined (analyst: A. Kounov) using the zeta approach (Hurford and Green, 1983) with a zeta value of 332 ± 7 for apatite

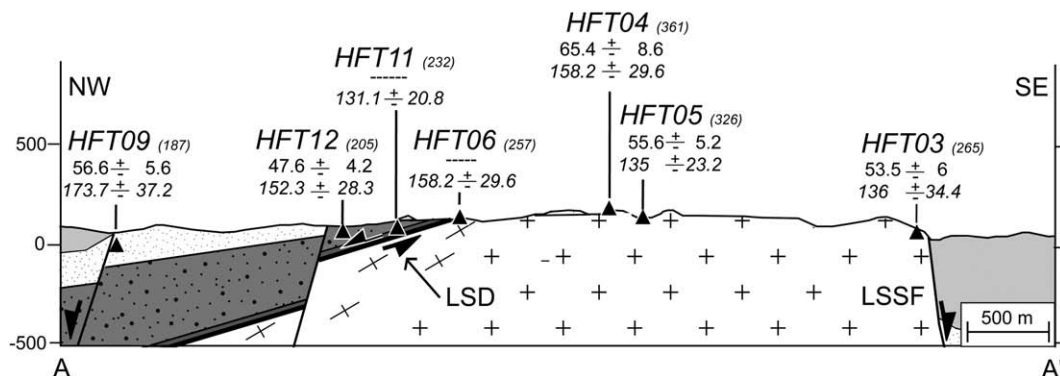


Fig. 4. Cross section across the La Serre Horst showing the fission track ages (central ages for apatite and zircon (italic); see also Table 1). Legend according to Fig. 3. LSD: La Serre Detachment; LSSF: La Serre Southern Fault.

Table 1

Sample details and results of zircon and apatite fission-track dating (refer to Figs. 3 and 4 for sample locations).

Sample number	Grid ref. UTM	Alt. m	Lithology	Strat. division	Mineral	Num. gr.	$\rho_d(\text{Nd})$ $\times 10^6 \text{ cm}^{-2}$	$\rho_s(\text{Ns})$ $\times 10^6 \text{ cm}^{-2}$	$\rho_i(\text{Ni})$ $\times 10^6 \text{ cm}^{-2}$	P(χ^2) (%)	Central age ($\pm 2\sigma$)Ma	MTL($\pm 2\sigma$) μm	S.D. (N) μm	Dpar μm
HFT02	709251/ 5233454	280	Marls	Toarcian	Zr	3	3.640(2659)	25.644(219)	2.459(21)	49	226.9 \pm 104.4			
HFT03	693894/ 5227481	265	Granite	Paleozoic	Ap Zr	20 5	15.397(8099) 3.591(2659)	1.838(1156) 22.764(486)	8.590(5403) 3.607(77)	0 65	53.5 \pm 6.0 136.4 \pm 34.4	12.68 \pm 0.25	2.6(104)	1.9
HFT04	693160/ 5229166	361	Sandstone	Triassic	Ap Zr	20 8	1.350(8099) 3.541(2659)	1.115(748) 23.217(1048)	3.611(2423) 3.124(141)	0 90	65.4 \pm 8.6 158.2 \pm 29.6	12.15 \pm 0.25	2.4(91)	2
HFT05	693001/ 5227873	326	Granite	Paleozoic	Ap Zr	20 8	1.461(8099) 3.516(2659)	1.314(783) 23.888(1122)	5.715(3406) 3.747(176)	58 100	55.6 \pm 5.2 135.0 \pm 23.2	12.10 \pm 0.23	2.4(106)	1.8
HFT06	694036/ 5230372	257	Granite	Paleozoic	Zr	12	3.442(2659)	18.073(1334)	2.859(211)	88	131.1 \pm 20.8			
HFT09	696691/ 5233176	187	Sandstone	Triassic	Ap Zr	20 7	1.3182(8099) 3.3182(2659)	0.890(714) 23.6014(907)	3.431(2752) 2.706(104)	74 97	56.6 \pm 5.6 173.7 \pm 37.2	12.50 \pm 0.23	2.4(103)	1.9
HFT11	691352/ 5229374	232	Rhyolithe	Permian?	Zr	7	3.269(2659)	20.323(781)	2.550(98)	95	156.6 \pm 34.6			
HFT12	691085/ 5229549	205	Sandstone	Permian	Ap Zr	20 9	1.429(8099) 3.195(2659)	0.981(923) 20.888(1134)	4.874(4586) 2.634(143)	97 100	47.6 \pm 4.2 152.3 \pm 28.4	12.89 \pm 0.26	2.6(101)	1.9

All ages are central ages (Galbraith, 1981). $\lambda D = 1.55125 \times 10^{-10}$. A geometry factor of 0.5 was used. $Zeta = 332 \pm 7$ for CN5/apatite and 122 ± 2 for CN1/zircon. Irradiations were performed at the OSU facility, Oregon State University Radiation Center, USA. $P(\chi^2)$ is the probability of obtaining χ^2 values for ν degrees of freedom where $\nu = \text{number of crystals} - 1$. ρ_d , ρ_s and ρ_i represent the standard, sample spontaneous and induced track densities respectively. MTL – mean track length. S.D.: standard deviation. Dpar: mean track pit length. All numbers in brackets are numbers of measurements.

(CN5 standard glass) and 122 ± 2 for zircon (CN1 standard glass). They are reported as central ages (Galbraith and Laslett, 1993) with a 2σ error (Table 1). The magnification used was $\times 1250$ for apatite and $\times 1600$ (dry objective) for zircon. Horizontal confined track lengths in apatite grains were measured at a magnification of $\times 1250$. Fission track etch pit diameters (Dpar) were measured at a magnification of $\times 2500$ in order to estimate the compositional influence on fission track annealing (Carlson et al., 1999).

The temperatures at which fission tracks in apatite and zircon minerals partially anneal (i.e. partial isotopic resetting) are not sharply defined. A temperature range, known as partial annealing zone (PAZ), exists where partial track annealing occurs. The track annealing leads to track lengths shortening and consequent age reduction. The effective closure of the system lies within this zone and is dependent on the overall cooling rates and the kinetic properties of the minerals. The heterogeneous annealing is a common feature for apatite and zircons from detrital sediments but also from some plutonic rocks as well (O'Sullivan and Parrish, 1995). Especially for detrital sediment samples, which have experienced only partial resetting (at temperatures lower than upper limit of the PAZ), wide spread of individual grain FT ages are characteristic. This is because the individual mineral grains are often coming from different source rocks and therefore have different kinetic properties due to their various chemistry or U content (see Tagami, 2005).

The specific partial annealing zone for apatite lies between 60 °C and 110 °C (Green and Duddy, 1989; Corrigan, 1993). Unfortunately our knowledge of zircon annealing is not as advanced as that of apatite and wide-ranging values for the temperature bounds for the partial annealing zone of zircon have been published. Yamada et al. (1995) suggest temperature limits of 170 °C to ~ 390 °C whereas Tagami and Dumitru (1996) and Tagami et al. (1998) suggested temperature limits of 230 °C to ~ 310 °C. Brandon et al. (1998) suggested lower than previously reported closure temperatures for natural α -damaged zircons. The main condition is that these samples have never experienced temperatures higher than the upper bound of the PAZ, which will cause the recovery of the accumulated through the time damages. Considering the relatively high amount of α -damage accumulated in the crystal lattice of the analysed samples, given the high protolith age (Variscan or older), we suggest temperature bounds for the zircon partial annealing zone (ZPAZ) between 160 and 270 °C as they have been calculated by Brandon et al. (1998) for the naturally α -damaged zircons. Accordingly we use a value of 215 °C

for positioning the ZFT central age in a temperature (T) vs. time (t) thermal history path (Section 6.1).

4. Results

4.1. Zircon

Eight samples from magmatic and sedimentary rocks were dated by the zircon FT method (Table 1). Due to the bad quality (metamictisation) of the majority of the zircon minerals from the samples analysed, only three to twelve datable grains were found per sample. Zircon central ages range from 227 ± 104 Ma to 131 ± 21 Ma (Table 1). All samples passed the χ^2 test and have FT ages younger than their stratigraphic ages, indicating that they were affected by temperatures higher than 160 °C after their deposition or formation. The only exception is the Liassic sample HFT02, from which only three grains could be dated; it has a central age that overlaps with the age of deposition, given its large 2σ error.

4.2. Apatite

Five zircon FT dated samples were also used for apatite FT analysis (Table 1). Apatite fission track central ages range between 65 ± 9 Ma and 48 ± 44 Ma. Three out of the five analysed samples (HFT05, HFT09 and HFT12) passed the χ^2 test. The samples have mean track lengths between 12.10 and 12.89 μm , with a standard deviation of 2.37–2.648 μm (Table 1). The Dpar values of the analysed samples range between 1.83 and 1.98 μm .

5. Subsurface analysis

The analysed seismic data cover an area east of the La Serre Horst known as the Avant-Monts Zone (Chauve et al., 1980; Madritsch et al., 2008; AMZ in Figs. 1, 3 and 5). The geological logs of deep wells (Fig. 6; see Figs. 3 and 5b for location) were obtained from BRGM (Bureau de Recherches Géologiques et Minières) Dijon office. Gaz de France provided seismic reflection sections (see Fig. 5b for locations). All seismic data have been commercially processed and were received for interpretation in the form of paper copies.

Seismic velocity analyses of the area were carried out based on correlations between two-way travel time (TWT) and stratigraphic logging in 4 deep wells (Fig. 6), as well as from seismic check-shot information from the surroundings of the wells. While high velocities

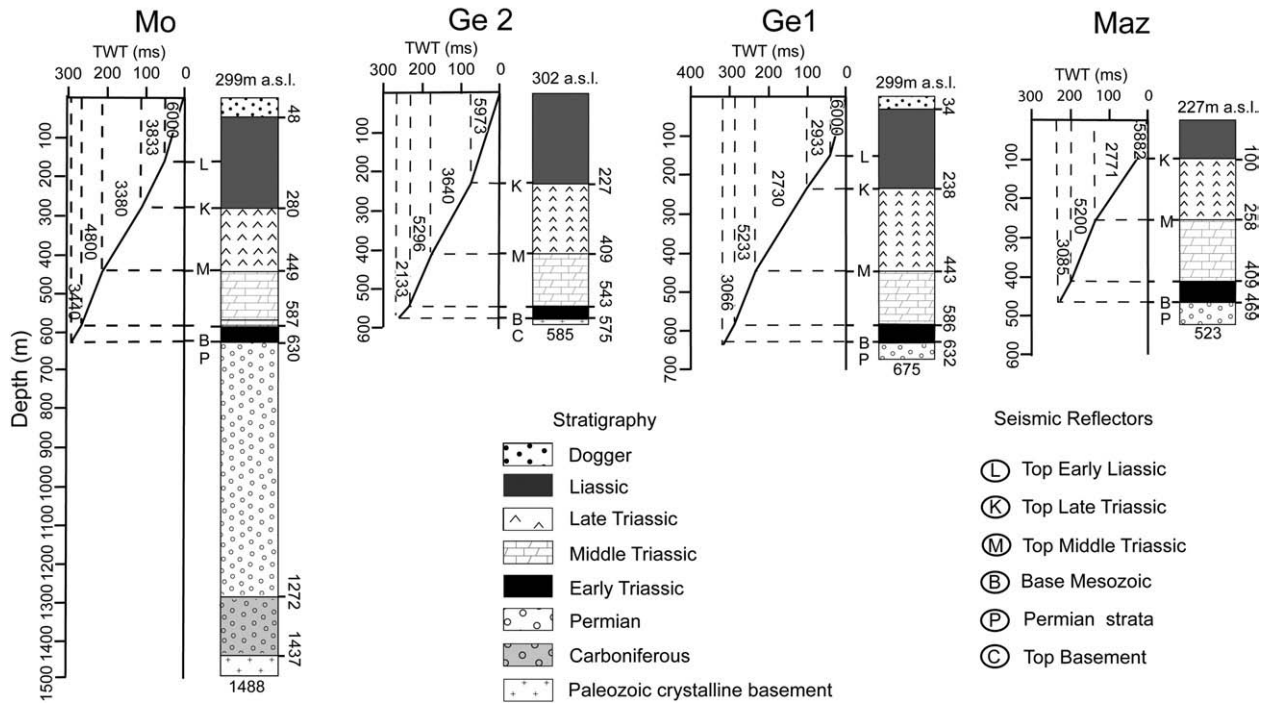


Fig. 6. Lithological logs of four deep wells from the Avant-Monts Zone, showing seismic interval velocities determined by correlation between seismic reflectors and depth of related stratigraphic horizons (see Figs. 3 and 5b for location). Note the position of the seismic reflectors outlined in Fig. 7.

indicative for an angular unconformity between Permo-Carboniferous sediments and overlying Mesozoic sediments (Fig. 7b–c). The contact between the Permo-Carboniferous deposits and the crystalline basement does not give rise to a clear reflector and thus is very difficult to define. However, in the vicinity of the LSH, the crystalline basement was reached by the Mo and Ge2 wells (Morre and Thiébaud, 1961; Figs. 3, 5b and 6) that are located near Line 1 (Fig. 7a) and Line 3 (Fig. 7c), respectively.

The seismic interpretations of a dense network of 10 seismic sections (Fig. 5b), combined with the borehole data (Fig. 6) and the available 1:50,000 geological maps (Chauve et al., 1983; Dreyfuss and Kuntz, 1969), allowed for the construction of a subsurface map at the level of the B-reflector, corresponding to the base of the Mesozoic series; the resulting TWT contour map is given in Fig. 5a. It illustrates the complex post-Paleozoic fault pattern adjacent to the La Serre Horst.

The NNE–SSW striking faults in the study area (Fig. 5) are mostly sub-vertical normal faults (Fig. 7a–c) and are oriented sub-parallel to the border faults of the Eocene–Oligocene Bresse Graben. The La Serre Southern Fault (Coromina and Fabbri, 2004; LSSF in Figs. 3, 4 and 5) shows a slightly different strike (NE–SW) and vertical offset of ~500 m. Paleozoic rocks are exposed in the La Serre Horst, i.e. in the footwall of the LSSF. Farther to the SE and in the hanging-wall of the LSSF (Figs. 6 and 8a) they are covered by a thick succession of Mesozoic sediments penetrated by well Ge2 (Morre and Thiébaud, 1961; Chauve et al., 1983; Figs. 6 and 7a). The base-Mesozoic boundary is well displayed in the seismic profiles (Fig. 7a–b). Its inclination to the NW, inferred from the subsurface map (Fig. 5a), indicates that the hanging-wall was slightly tilted towards the LSSF.

The fault set striking ENE–WSW runs parallel to the Late Paleozoic Burgundy Trough (Figs. 2 and 5). The most prominent faults of this set are the Ognon, Avant-Monts and Arne faults (OGF, AMF and AF respectively, indicated in Fig. 5a). Generally these faults show more gentle dips and greater vertical offsets than the NNE–SSW striking ones (Fig. 7b and d).

The above-described faults often represent reactivated Late Paleozoic faults. This reactivation can be inferred from the seismic

sections depicted in Fig. 7. In the central part of Lines 1 and 2 (Fig. 7a,b) the Mesozoic sediments form several gentle flexures. Slight flexuring of the Mesozoic is visible above the NNE–SSW striking eastern border fault (LSB) of the La Serre Horst Structure (inset of Fig. 7a featuring a detail). Flexuring is much more pronounced above the ENE–WSW-striking normal faults (e.g. the Arne Fault Fig. 7b and d) where reactivation is clearly extensional (Fig. 7a–c). Such normal faults also form the northern and southern boundaries of the Late Paleozoic La Serre Horst Structure.

Some of the normal faults have been reactivated in a compressive to transpressive mode during a later stage of deformation. The best example for later inversion is the Avant-Monts Fault (AMF in Fig. 7d). This steep reverse fault is closely related to an adjacent and ENE–WSW-oriented graben (Figs. 5b and 7d), strongly suggesting that it is an inverted normal fault.

6. Brittle deformation and paleostress analysis

6.1. Methodology

To assess the kinematic history of post-Jurassic brittle deformation along the RBTZ and to document the control exerted by the pre-existing Paleozoic La Serre Horst Structure on its Cenozoic tectonic evolution we applied a combined kinematic–dynamic paleostress determination based on fault slip data analysis (Angelier and Mechler, 1977; Marrett and Allmendinger, 1990; Pfiffner and Burkhard, 1987). Analyses were carried out at 56 different sites throughout the entire RBTZ giving more than 2400 individual fault slip measurements.

Measurements were predominantly carried out on Middle (Bajocian) to Latest Jurassic limestones (Sequanian) in the whole study area and locally on Late Paleozoic granites (sites 48, 49), Permian conglomerates and volcanics (site 47), as well as on Middle Triassic limestones (Muschelkalk formation, site 8). Slickolites were the most frequent slip indicators found. Calcite slickenfibres and lunate fractures (Petit, 1987) were only occasionally detected. The kinematic indicators were given quality marks (Table 2) ranging from 1 (excellent) to 3 (poor). A chronology of brittle faulting was established in the

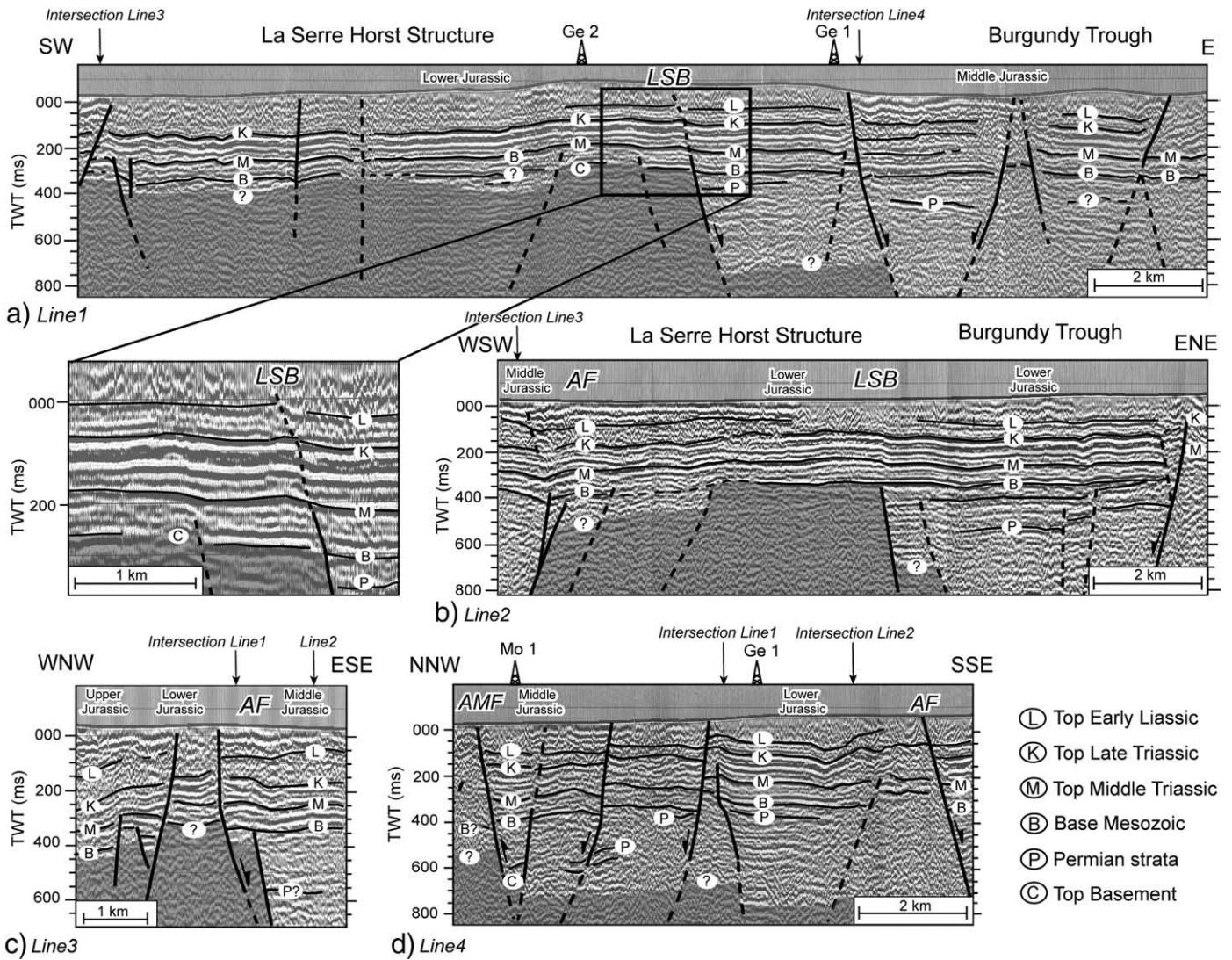


Fig. 7. Selected seismic reflection lines across the Avant-Monts Zone. See Fig. 5b for the location of the lines and Fig. 6 for well logs and stratigraphic identification of seismic reflectors. AF: Arne Fault; AMF: Avant-Monts Fault; LSB: La Serre Border Fault. a) Line 1, crossing the subsurface border of the La Serre Horst Structure that is documented by boreholes Ge1 and Ge2 and that appears to be slightly reactivated, as is indicated by the flexure of the overlying Mesozoic strata (see inset). b) Line 2, parallel to Line 1, but also crossing the Arne Fault in the western part of the section, where a pronounced extensional flexure is developed. c) Line 3, extending from the La Serre Southern Fault, not displayed on the section, all the way across the Arne Fault. d) Line 4, displaying the Avant-Monts Fault, a steep reverse fault that emerges out of a Paleogene/Late Paleozoic graben and is inferred to have formed by inversion of a former normal fault. The southern part of this section crosses the Arne Fault.

field by the observation of overprinting relationships between different striae on the same fault plane, or alternatively, by crosscutting relationships between different fault sets (Fig. 8).

The field data were processed with the Windows-based computer program TectonicsFP (Reiter and Acs, 1996–2000). Data sets from each locality were first separated into homogeneous subsets, based on overprinting and/or crosscutting criteria observed in the field (Figs. 8 and 9a). In addition, we applied the pole projection plot (Meschede and Decker, 1993) and the p–t axes method (Marrett and Allmendinger, 1990) in order to graphically test the fault sets for kinematic homogeneity (Fig. 9b). Thus, kinematically incompatible fault-striation pairs could be detected within a given subset and be reconsidered as part of another subset, taking also into account the quality of the slip indicators.

In addition to the kinematic analyses based on the p–t axes method (Marrett and Allmendinger, 1990) we also applied the dynamic Right-Dihedra method (Angelier and Mechler, 1977; Pfiffner and Burkhard, 1987; Fig. 9c). While the first method is purely descriptive and calculates the principal axes of incremental strain (Marrett and

Peacock, 1999), the latter permits to estimate the orientation of the principal axes of stress ($\sigma_1 > \sigma_2 > \sigma_3$; Angelier, 1989). P–t axes and Right-Dihedra methods revealed similar results regarding the orientation of incremental strain and the principal stress axes, respectively (Fig. 9b–c).

All paleostress methods rely on several assumptions, the most important ones being that (i) slip observed on a fault plane is parallel to the maximum resolved shear stress (Wallace, 1951), (ii) movement on a fault occurred under a homogenous state of stress and (iii) faults do not mechanically interact with each other. The Right-Dihedra method is the most simple paleostress analysis and does not calculate a stress ratio. However, it is considered the most robust paleostress method that is particularly suited for areas undergoing poly-phase brittle deformation, and it was found to be less sensitive to highly asymmetric fault plane associations (Meschede and Decker, 1993). The Right-Dihedra method only delivers an estimation of the possible orientation of the principal stress axes with the most likely orientation computed at point maxima of superimposed compressional and tensional dihedras, calculated for each fault slip pair (Angelier and

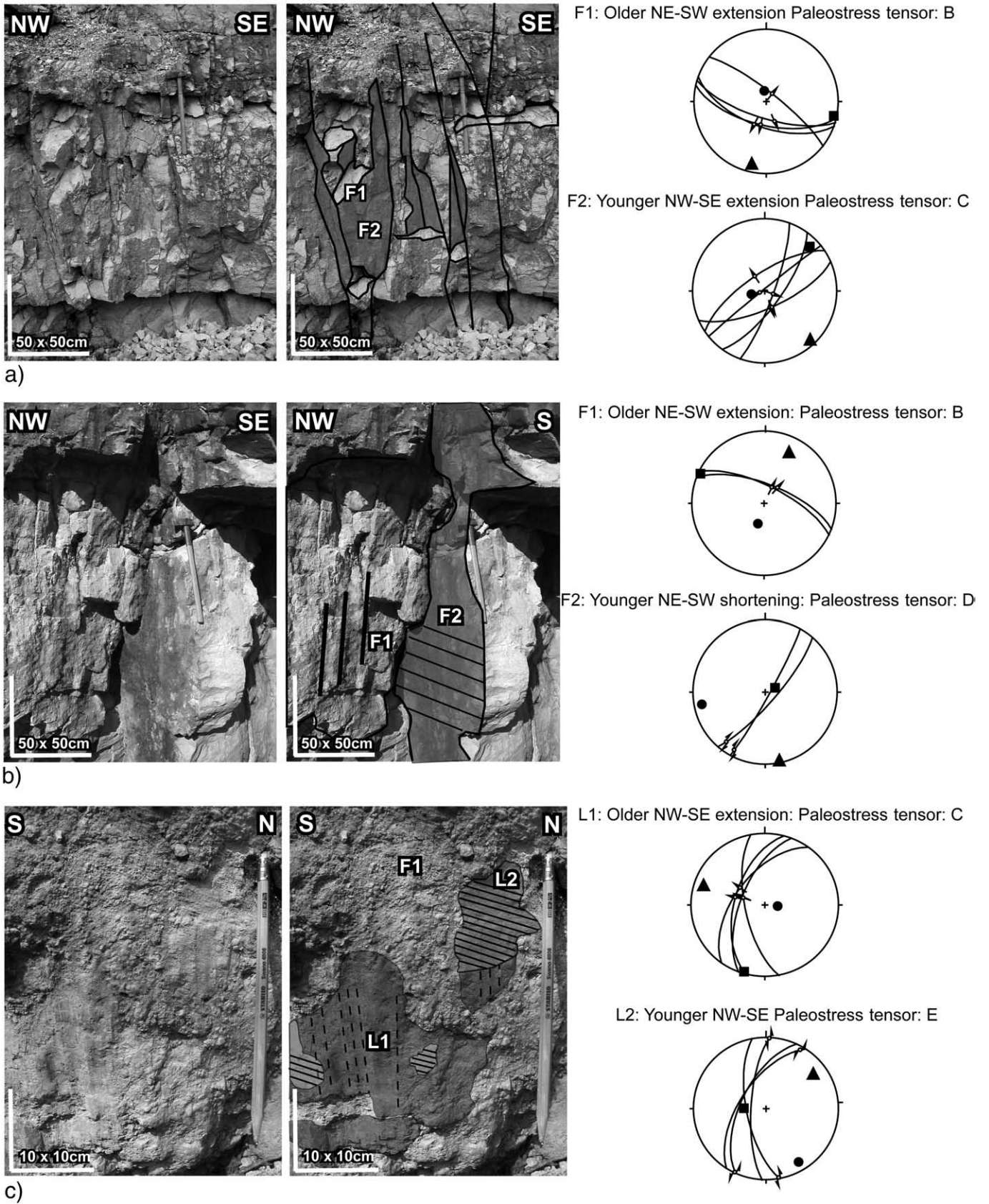


Fig. 8. Examples of crosscutting and overprinting criteria of brittle structures, allowing to distinguish different deformation stages and to establish a relative chronology. Stereographic, equal area, lower hemisphere projections of the fault slip data are also shown (circles, squares and triangles indicate σ_1 , σ_2 , and σ_3 , respectively). a) Crosscutting generations of normal faults. b) Steep strike-slip faults indicating ENE–WSW shortening and crosscutting older normal faults. c) Strike-slip slickolites overprinting a former normal fault.

Table 2 (continued)

Site	Location	X	Y	Age	Tensor	σ_1		σ_2		σ_3		N	n	Q
						Azi.	Pl.	Azi.	Pl.	Azi.	Pl.			
35	Chemaudin	869683	2251673	Bathonian	34 e	169	1	30	88	259	1	11	4	2
					35 a	196	10	324	74	104	13	22	9	1
					35 c	277	88	34	1	124	2	9	2	2
36	Rouset Fluans	864477	2247181	Sequanian	35 e	112	7	339	80	203	7	44	7	2
					36 d	228	2	32	87	137	1	7	2	2
37	StVit East	865082	2248531	Bathonian	37 a	178	6	32	83	268	4	13	7	3
					37 b	245	55	142	9	46	34	8	0	1
					37 e	126	2	13	86	216	4	24	11	2
38	StVit West	861106	2247349	Bajocian	38 c	221	82	50	8	320	1	13	2	
					39 c	296	53	204	1	113	37	28	0	1
39	Avrigney	859725	2266975	Sequanian	40 a	198	7	45	82	288	4	22	1	1
					40 e	325	15	115	73	233	8	20	8	1
40	Marnay	857676	2261435	Rauracian	41 b	230	58	138	1	47	32	15	7	1
					41 c	55	83	186	5	277	5	17	7	1
41	Ranchot	837564	2244604	Bathonian	41 d	255	3	41	86	165	2	29	9	2
					41 e	150	2	311	88	60	1	8	4	1
					42 b	206	56	302	4	35	34	4	0	1
42	Monteplain	855656	2244379	Callovian	42 c	185	61	72	12	336	26	8	2	2
					42 d	71	6	330	63	164	27	13	0	2
					42 e	167	12	5	76	256	3	31	4	2
43	Taxenne	853637	2252571	Bajocian	43 b	216	84	109	2	19	6	9	4	3
					43 c	147	74	249	4	340	16	7	x	1
					43 e	295	13	171	65	30	19	14	5	1
44	Gendrey	852178	2251000	Bathonian	44 c	339	82	237	2	147	8	6	1	1
					44 e	118	2	223	82	28	7	75	28	3
					45 b	125	64	278	23	12	11	30	6	1
45	Montagney	852290	2258967	Sequanian	45 c	316	67	215	4	123	23	39	5	1
					45 e	299	5	45	74	208	15	12	2	3
					46 b	189	60	325	22	63	19	9	1	2
46	Brans	845366	2252501	Bajocian	46 c	59	61	192	21	289	20	7	0	2
					47 a	355	5	161	85	265	1	12	3	1
					47 b	78	71	311	12	218	15	13	2	1
47	Moissey	843650	2249429	Permian Vulcanite	47 d	58	2	255	8	148	1	13	4	3
					47 e	333	7	181	82	64	4	27	7	2
					48 c	18	59	218	29	123	9	5	2	3
48	Bois deMalange	847016	2248868	Paleozoic Granite	40 b	133	39	341	48	234	14	13	6	3
					40 e	330	7	81	71	238	17	18	8	1
					50 d	236	5	20	83	146	4	13	1	2
50	Orchamp	849709	2243594	Bathonian	50 e	327	1	220	88	57	2	36	20	1
					51 b	219	66	114	7	21	23	9	2	1
					51 c	120	71	233	8	326	17	10	3	1
51	Amange	844435	2246175	Bajocian	51 e	340	7	82	61	246	28	15	6	2
					52 c	217	54	24	35	118	7	6	2	2
					52 d	63	14	228	75	332	4	6	2	2
52	Jouhe	839834	2242920	Bajocian	52 e	151	5	260	76	60	13	12	6	1
					53 b	171	61	272	6	5	28	12	6	2
					53 c	250	73	35	15	128	10	28	9	1
53	Authume	839385	2239778	Bathonian	53 d	69	2	322	83	159	6	22	6	2
					53 e	152	6	31	78	243	10	35	18	1
					54 c	287	56	27	7	122	33	23	10	1
54	Mont Roland	837702	2239442	Bathonian	54 c	247	4	142	76	338	13	17	7	3
					54 d	56	51	308	14	208	36	12	6	2
					54 e	166	5	46	76	247	14	26	12	1
55	Monniere	837702	2238544	Bajocian	55 a	194	5	52	84	284	4	32	15	1
					55 b	296	65	111	25	202	2	23	8	1
					55 c	268	54	16	12	114	34	37	7	1
55	Dampiere	834224	2234180	Sequanian	55 d	261	5	103	84	351	2	19	2	2
					55 e	140	10	26	68	234	20	18	3	1
					56 a	185	5	51	83	276	5	14	1	2
56	Dampiere	834224	2234180	Sequanian	56 b	216	49	102	20	368	34	8	4	2
					56 c	139	70	46	1	316	20	16	6	1
					56 d	46	1	189	88	316	1	10	1	1
56	Dampiere	834224	2234180	Sequanian	56 e	148	6	51	52	243	37	20	3	1

Numbers and letters refer to locations and deformation stages, respectively, as given in Fig. 10. $\sigma_1, \sigma_2, \sigma_3$: maximum, intermediate and minimum principal stress axes; Azi.: azimuth; Pl.: plunge; N: number of measured faults considered for paleostress calculation; n: number of faults with no indication of slip direction; Q: Quality remark (1: excellent; 2: good; 3: poor).

Mechler, 1977; Pfiffner and Burkhard, 1987; Fig. 9c). Therefore the Right-Dihedra method considers also movements along possibly pre-existing, reactivated fault planes that are not ideally oriented in respect to a theoretical best-fit reduced stress tensor calculated when applying Direct Inversion methods (Angelier, 1990).

6.2. Results

The results of paleostress analyses are illustrated in Fig. 10 and Table 2. In addition, lower hemisphere equal area projections of all fault-slip datasets are shown in the electronic appendix that is

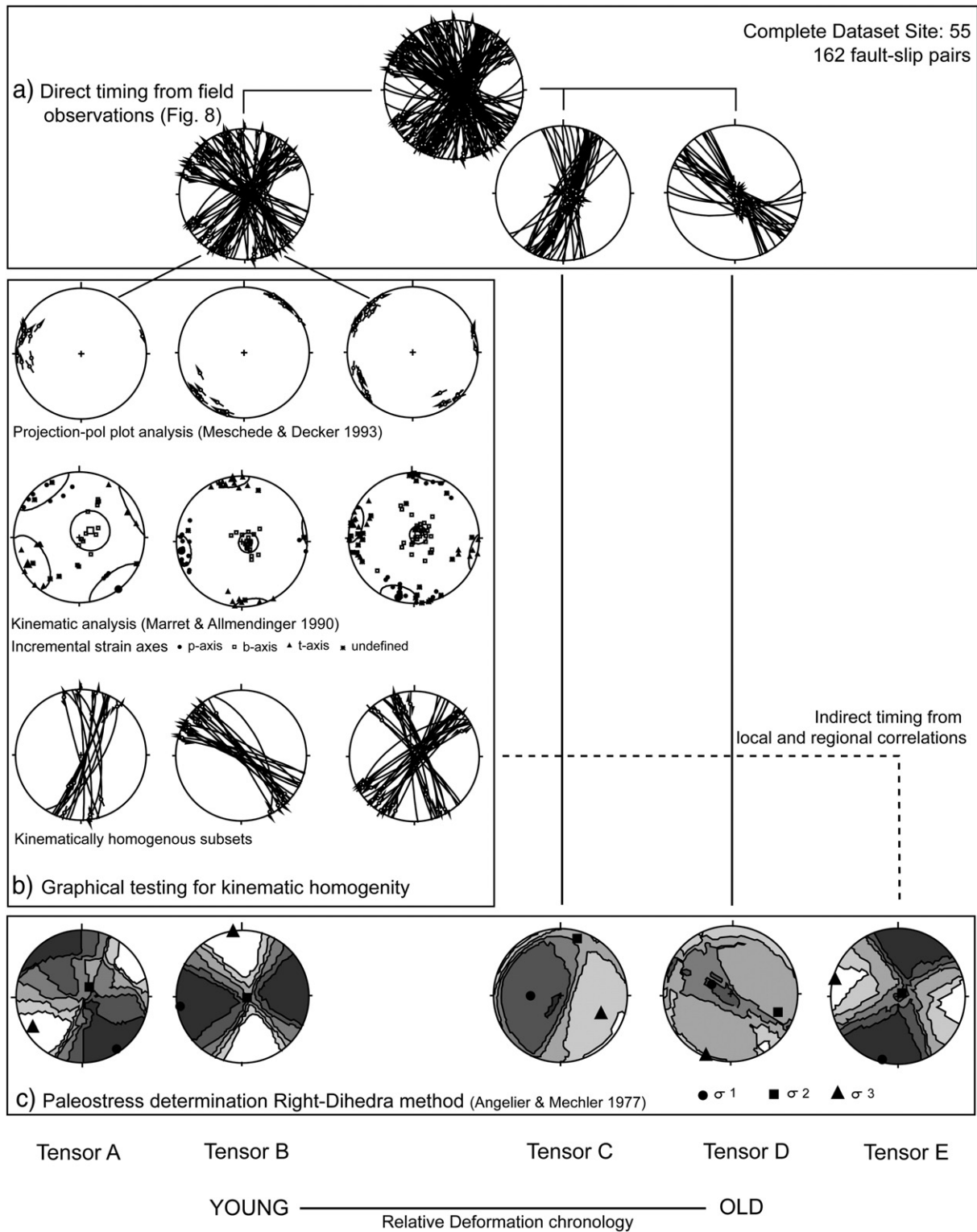


Fig. 9. Processing of fault-slip data. Fault slip data shown as stereographic, equal area, lower hemisphere projections. a) Field observations provide the first order criteria for separating the dataset into different deformation events. b) Graphical tests applied for further separating the remaining dataset into homogenous subsets prior to paleostress analysis. c) Paleostress analysis using the Right-Dihedra method, as applied to kinematically homogenous subsets in order to establish the related stress tensor by estimating the orientation of the principal stress axes ($\sigma_3 < \sigma_2 < \sigma_1$).

accessible via the online version of this publication (also see Madritsch, 2008). Five different kinematically homogeneous fault sub-sets were detected. From these sub-sets five distinct stress tensors, related to the post-Jurassic stages of brittle deformation, were calculated (stress tensors A–E in Fig. 9). Their relative chronology is established by the observation of crosscutting and

overprinting structures, and additionally supported by correlation with previous studies from neighbouring areas (Bergerat, 1987; Larroque and Laurent, 1988; Lacombe et al., 1990, 1993; Homberg et al., 2002; Rocher et al., 2003; Ustaszewski et al., 2005a; Lopes-Cardozo and Behrmann, 2006; Figs. 8 and 9c). Due to the limited number of available observation sites within Late Paleozoic and

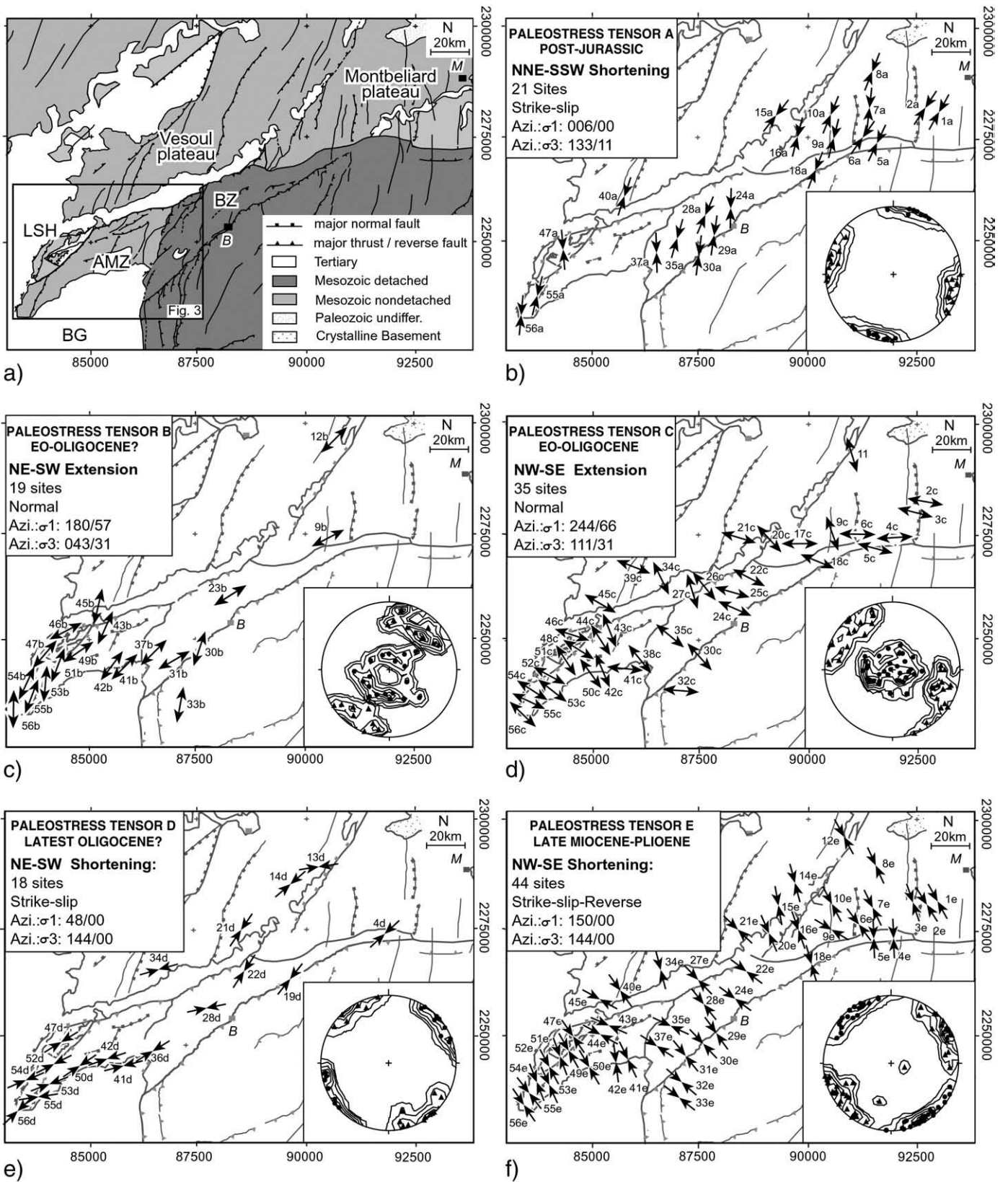


Fig. 10. Paleostress maps for the Rhine–Bresse Transfer Zone displaying 5 different paleostress tensors. Convergent and divergent arrow pairs indicate the orientation of maximum (σ_1) and minimum (σ_3) axis of principal stress, respectively, as obtained using the Right-Dihedra method (compare Table 2). Insets show contoured equal area lower hemisphere projections of the calculated tensors from each site with circles indicating σ_1 and triangles indicating σ_3 . a) Tectonic map of the area (tectonic units after Madritsch et al., 2008). b) Post-Jurassic NNE-SSW shortening. c) NE-SW extension of presumed Eocene–Oligocene age, occurring locally around the La Serre Horst. d) NW-SE extension of Eocene–Oligocene age. Note the systematic deflection of the extension direction. e) NE-SW shortening, postdating Eocene–Oligocene extension. f) NW-SE shortening representing the youngest deformation event recorded.

Triassic formations (sites 8, 47, 48, 49, compare Table 2) it was not possible to establish any reliable pre-Jurassic paleostress tensors.

Fig. 10 shows the regional distribution of the five paleostress tensors. The arrows in Fig. 10 indicate the azimuth of the axis of either the maximum (σ_1) or the minimum (σ_3) principal stress, as derived from the Right-Dihedra paleostress analysis for each site (Fig. 9c). In addition, contoured projections of all tensors (σ_1 as circles, σ_3 as triangles) obtained for a particular phase are shown. From the orientation of σ_1 and σ_3 the tectonic regime can be inferred.

Paleostress tensor A is obtained from the relatively oldest fault set consisting of strike-slip faults. It indicates NNE–SSW-directed compression (Figs. 9 and 10b). These strike-slip faults are commonly reactivated as normal faults that define NE–SW and NW–SE directed extension (paleostress tensors B and C respectively, Fig. 10c–d).

Paleostress tensor B, indicates NE–SW extension, is observed exclusively around the northern border of the Bresse Graben (BG) and the La Serre Horst (LSH) whereas the paleostress tensor C (Fig. 10d) is recorded throughout the entire RBTZ. The latter tensor is constrained by NNE–SSW to ENE–WSW striking normal faults. σ_3 shows a relative change in its orientation along the studied area (Fig. 10d). The extension direction is oriented WNW–ESE in the eastern part of the study area and progressively rotates into a NW–SE, locally a NNW–SSE, orientation in the western part including the LSH area. Occasionally the normal faults that define paleostress tensor B were found to be overprinted by normal faults associated with paleostress tensor C (e.g. sites 53, 55, 41; Fig. 8a). However, relative overprinting criteria between these two fault sets could not be consistently detected at all sites and remained ambiguous.

Both sets of normal faults are overprinted by a set of strike slip faults (Fig. 8b) that define a paleostress tensor indicating NE–SW compression (stress tensor D, Fig. 10e). This sub-set of faults was only detected at a limited number of sites (e.g. sites 9, 10, 41, 45, 53, 54, 55; Fig. 10e).

The youngest sub-set of faults defines a paleostress tensor indicating NW–SE directed compression (paleostress tensor E in Figs. 9 and 10f) and was recorded in almost all of the investigated sites (Table 2). In the field it is manifested by strike-slip reactivation of

pre-existing NNE–SSW and WNW–ESE striking normal faults (Fig. 8c), as well as by newly formed thrust faults along the northwestern front of the thin-skinned Jura fold-and-thrust belt discussed in Madritsch et al. (2008).

7. Data interpretation and discussion

7.1. Exhumation history of the La Serre Horst

The combination of fission track analysis with structural data allows constraining the thermal and tectonic evolution of the La Serre Horst (LSH) since the Paleozoic and in the context of the evolution of the European Cenozoic Rift System (Fig. 11). Field data indicate that the exhumation of the La Serre Granite along the low-angle La Serre Detachment started during or shortly after granite intrusion at around 317 ± 5 Ma (Coromina and Fabbri, 2004; Choulet et al., 2007; Choulet pers. communication). Crustal extension of the same age accompanied by granite emplacements is also observed in the Black Forest, the Vosges Mountains and the Massif Central (Fig. 1) and is possibly related to magmatic underplating and/or orogenic collapse (Eisbacher et al., 1989; Echtler and Malavielle, 1990; Echtler and Chauvet, 1991–1992; Rey et al., 1991–1992). Therefore we assume the La Serre Granite to be part of a Late Paleozoic metamorphic core complex that partially crops out today in the La Serre Horst (LHS in Fig. 2).

Extension in this core complex continued in Late Carboniferous and Permian times, accommodated by high angle, brittle normal faults. This later stage of extension led to the formation of the Burgundy Trough and the La Serre Horst Structure (LSHS in Fig. 2). Low- and high-angle normal faulting ceased sometime before the Early Triassic, as shown by the fact that the Permian horst and graben structures are sealed by Lower Triassic strata (Coromina and Fabbri, 2004; Figs. 4, 7a–b and 11). Similar observations were made elsewhere in Western Europe (Ziegler, 1990; Ziegler et al., 2004; McCann et al., 2006).

The further Mesozoic thermo-tectonic evolution of the study area was revealed through our zircon and apatite fission-track thermo-chronological data. The zircon fission track analyses of the Variscan

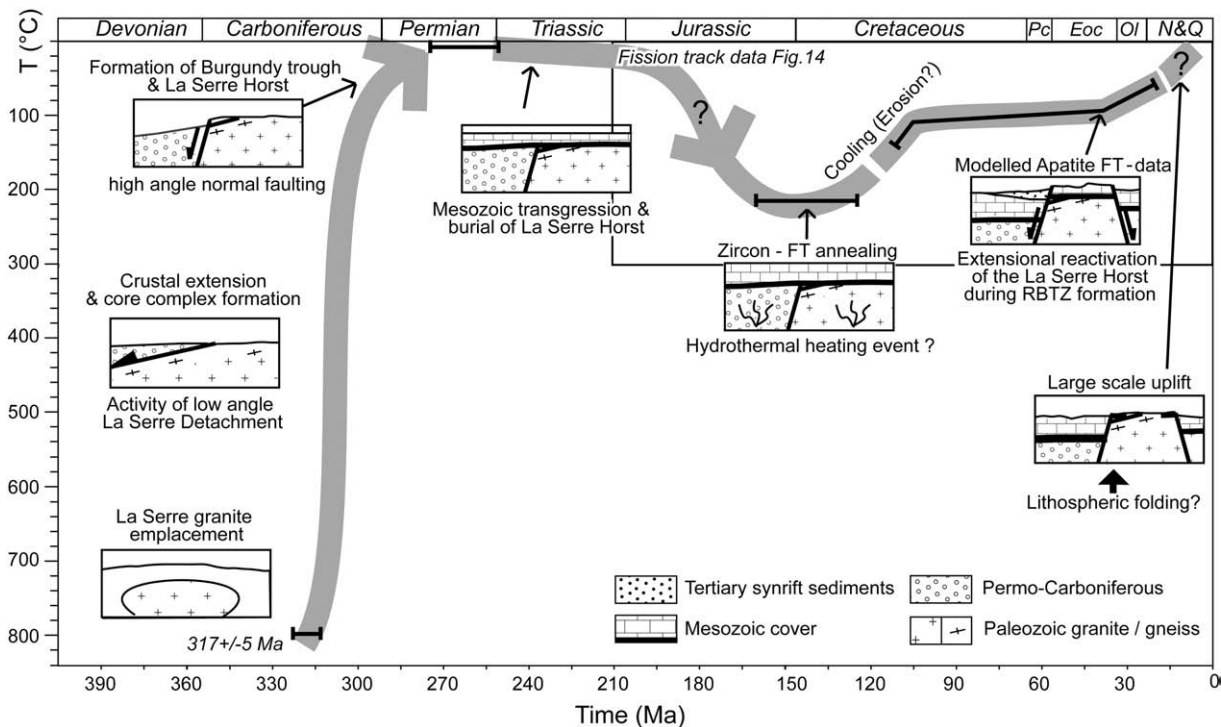


Fig. 11. Exhumation history of the La Serre Horst as inferred from fission-track and structural data.

basement of the La Serre Horst and its Permian to Lower Triassic cover indicate that these rocks have experienced a substantial amount of annealing, as indicated by the reduction of the central ages with respect of their emplacement or deposition ages (Fig. 11). Sample HFT02, a Toarcian claystone, is the only exception (Fig. 3; Table 1). Among the three analysed zircon grains from this sample two have ages older than the stratigraphic age and one is overlapping within the 2σ error. Therefore this sample experienced only little, if any, annealing since its deposition and remained at a shallower depth than the other samples. Hence, it will not be used in the following discussion on the thermal evolution of the area.

Unfortunately, it is very difficult to estimate the exact temperatures at which the zircon fission tracks in the analysed samples were annealed. The large spread of single grain ages (Fig. 12) obtained for the analysed samples could be explained by the different degrees of annealing which zircon grains experienced due to their different kinetic properties at temperatures probably below the upper temperature limit of the partial annealing zone (270 °C). This suggestion is in line with the previously reported maximum temperatures of 200–250 °C, which the Mesozoic sedimentary cover and underlying basement have experienced in the URG area (Brockamp and Zuther, 1983; Surma et al., 2003; Timar-Geng et al., 2004).

The high $P(\chi^2)$ values obtained from the analysed samples (higher than 5%) and the respective absence of extra-Poissonian variation of the single grain age distribution does not necessarily indicate that they belong to the single age population (see Green, 1981) but is rather a consequence of poor statistics due to the low number of counted tracks. Therefore we conclude that the large spread in single grain ages is related to the different track retentivities of the individual grains within a given sample. Moreover, a relationship between lithology and FT ages is also observed. The three granite samples show younger ages (between 131 ± 21 and 136 ± 34 Ma) when compared to the sedimentary and volcanic samples (between 152 ± 28 and 173 ± 37 Ma, again excluding sample HFT02). Although the annealing characteristics of zircon are still poorly understood, the distinct annealing behaviour was probably related to variable amounts of accumulated α -damages and/or compositional variations. The exact timing of the heating event that led to the annealing of the analysed samples is also difficult to be determined. We suggest that this event is most probably of Late Jurassic–Early Cretaceous age (Fig. 11). This is the time span for which the zircon single grain age distribution shows a maximum (130–160 Ma, Fig. 12), possibly implying that the temperature obtained within ZPAZ was a maximum during this period of time. After 110 Ma the analysed samples already reached temperatures that are within the apatite partial annealing zone (less

than 110 °C), as is indicated by the apatite single grains that reach ages up to 110 Ma (Fig. 12).

The total maximum thickness of the Mesozoic sediments, including eventually eroded parts, is estimated to range between 2200 and 2500 m, based on well data (Fleury et al., 1982; Chauve et al., 1983) and the fission track analyses along the crystalline flanks of the Southern Upper Rhine Graben (Timar-Geng et al., 2006) and the southern French Massif Central (Barbarand et al., 2001). Therefore, we assume that during this heating event the rocks analyzed in this study were at a maximum depth between 1300 and 2500 m. This implies that our FT results indicate an anomalously high thermal gradient that cannot be explained by burial alone. Similar elevated thermal gradient, presumably due to hydrothermal fluid activity during the Jurassic and Early Cretaceous, was reported for the Variscan basement and its Mesozoic cover from the French Massif Central (Macquar, 1984; Lancelot et al., 1995) and from north-western Switzerland, including the area of the southern Upper Rhine Graben (Wetzel et al., 2003; Timar-Geng et al., 2004; Timar-Geng et al., 2006). Although the thermal pulse is reported as being related to hydrothermal fluid migration, it apparently affected a large area comprising the entire central part of the European Cenozoic Rift System (Timar-Geng et al., 2006). Wetzel et al. (2003) tentatively relate such hydrothermal processes (from Sinemurian to Oxfordian times) to phases of tectonically induced enhanced subsidence during crustal extension in the continental margin of the Alpine Tethys. However, such hydrothermal activity may only be a consequence rather than the main cause of the regionally elevated thermal gradient whose cause is still not well understood. It is most likely related to some mechanism of heat transfer from the mantle.

The later thermal evolution of the La Serre Horst is constrained by apatite fission track data. The analysed samples have relatively short mean track lengths (between 12.10 and 12.89 μm ; Table 1) with broad and often bimodal distributions (Fig. 12). Broad track length distributions, combined with shorter mean lengths, suggest that the samples experienced a complex thermal history and that they spent a significant amount of time within the PAZ for apatite (Gleadow et al., 1986). We modelled the apatite fission track data in order to quantify timing and amount of cooling experienced by the samples analysed as they remained within the apatite PAZ (Fig. 13). Modelling of the apatite ages and the track length distribution data was completed with the Monte Trax program of Gallagher (1995), using an initial track length of 16.3 μm . A composition of Durango apatite was used with the Laslett model when running modelling programs.

The zircon FT central ages, combined with the thermal evolution models on the basis of the apatite data, reveal a thermal history that is characterized by two distinct periods of cooling since Late Jurassic times (Fig. 13). A first cooling event occurred during the Early Cretaceous (Figs. 11 and 13) and is probably related to thermal relaxation that occurred after hydrothermal activity in the area had ceased. Some of this cooling could also be attributed to erosional denudation, as it is suggested by the presence of intra-Cretaceous unconformities in the area (Chauve et al., 1983). This cooling was followed by a Late Cretaceous to Early Cenozoic period of relative quiescence for which only extremely slow cooling rates are inferred (Figs. 11 and 13). The only exception to this is sample HFT09, which still experienced relative cooling to a temperature of less than 80 °C during this same period of time (Fig. 13). Data modelling predicts that a relatively high geothermal gradient was maintained all the way to the Early Paleogene. However, it must be pointed out, that relative variations in the temperatures estimated by the modelling in the order of ± 30 °C need to be considered to account for the dependency of the track annealing process on the apatite composition, in particular the Cl/F ratio (Green et al., 1985, 1986; Burtner et al., 1994).

A second, well-pronounced and relatively fast cooling event started some 38 to 32 Ma ago (Fig. 13). Since the start of this cooling event coincides rather well with the onset of syn-rift deposition in the

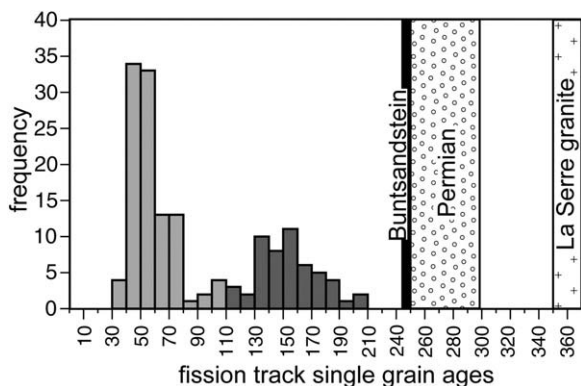


Fig. 12. Frequency distribution of the apatite (light grey) and zircon (dark grey) single-grain ages from the analysed samples. Also shown are the ages of emplacement or deposition, respectively, for the samples (compare Table 1). Note that sample HFT02 is not considered.

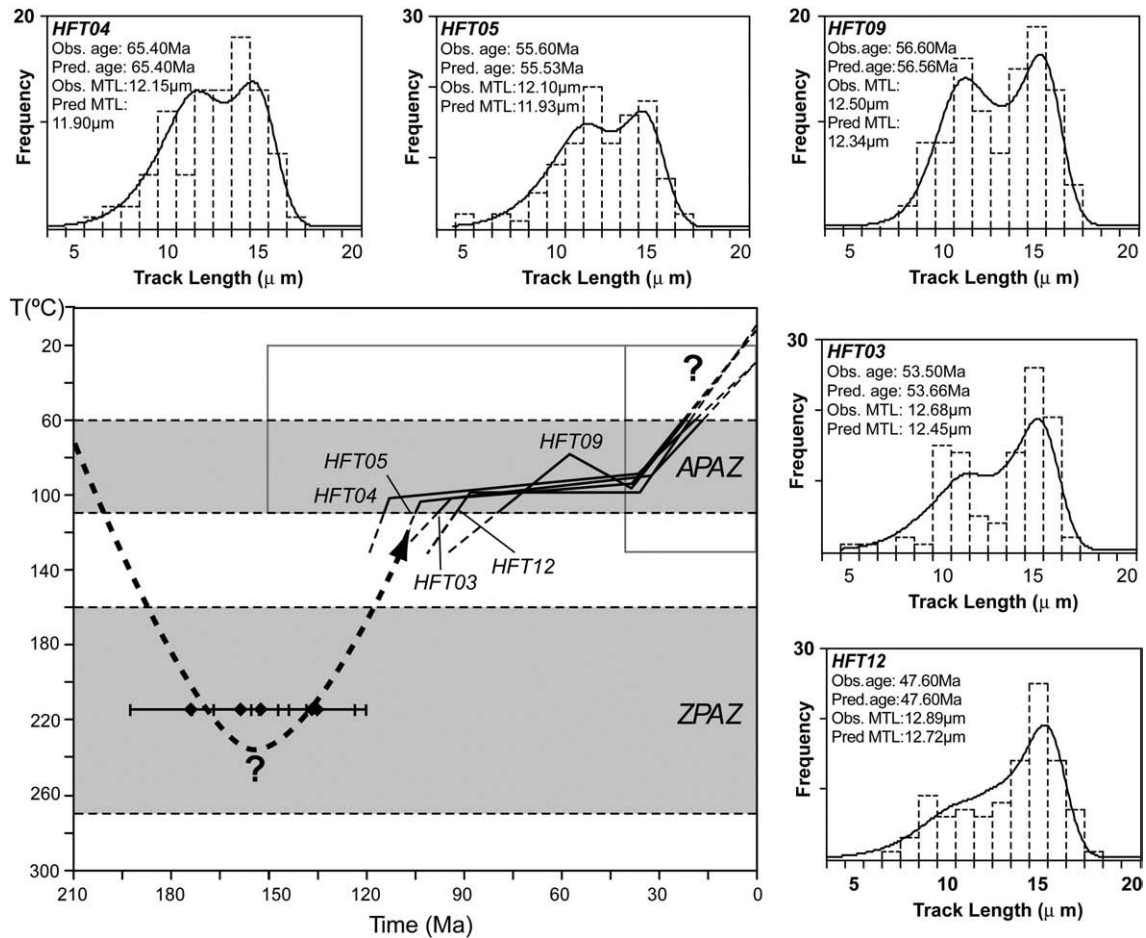


Fig. 13. Modelled thermal history and comparison between observed and predicted fission track parameters for the individual FT samples from the La Serre Horst. The upper left corner of the model diagrams compares the observed ages with those predicted by the model; also given are the observed and predicted mean track lengths (MTL). The thick black lines in the model diagrams represent the best-fit model. The apatite partial annealing zone (APAZ) lies within the temperature limits assigned by Laslett et al. (1987). The dashed segments of the thermal histories at temperatures lower than 60 °C only indicate a possible continuation of the thermal history because the annealing model is not sufficiently sensitive below 60 °C. The modelled T-t paths are extended into the zircon partial annealing zone (ZPAZ following Brandon et al., 1998) where the black diamonds represent the zircon FT ages for the modelled samples. See Figs. 3 and 4, and Table 1 for more details on the samples.

URG (Middle to Late Eocene 42.5–36 Ma, Berger et al., 2005; Hinsken et al., 2007), it is interpreted as a consequence of accelerated erosion in the La Serre Horst Structure due to extension and rift shoulder uplift. Eocene to Oligocene cooling related to rifting was also suggested by Timar-Geng et al. (2006), based on apatite fission track modelling on crystalline samples from the flanks of the southern Upper Rhine Graben. Most importantly, this second cooling event indicates that the La Serre Horst, already formed in Permian times, was substantially reactivated during Eo-Oligocene rifting; hence it must be considered as an active horst structure also during this tectonic phase. Sample HFT09, collected near to the main border fault delimiting the La Serre massif to the north (Ognon Fault, Fig. 3), shows some late heating with its temperature maximum being attained at about 38 Ma (Fig. 13). This heating could possibly be related to the hot fluids circulating along the fault while it was active.

In summary, the fission track data presented in this study show that substantial exhumation of the La Serre Horst Structure started during Cenozoic rifting, i.e. before the end of the Oligocene (~23 Ma). However, the fission track data do not constrain the timing of final exhumation of the rocks to the earth's surface (Figs. 11 and 13). This last cooling event was probably driven by large-scale Early Miocene uplift of the northwestern Alpine foreland due to lithospheric deformation induced by the Alpine collision (Dèzes et al., 2004; Bourgeois et al., 2007; Ziegler and Dèzes, 2007; Fig. 11). Thick-skinned dextrally transpressive reactivation of the Rhine-Bresse Transfer Zone in Early Pliocene to recent times (Madritsch et al., 2008) could also

have contributed to the final exhumation of the La Serre Horst that forms a restraining bend in such a tectonic setting.

7.2. Structural grain of the western Rhine-Bresse Transfer Zone

We now discuss the relationships between the Late Paleozoic Burgundy Trough, the La Serre Horst Structure (Fig. 2) and the Post-Jurassic fault pattern as recorded in the Mesozoic cover. Our interpretation is based on the base-Mesozoic (B reflector) contour map presented in Fig. 5a and two interpretative structural cross-sections given in Fig. 14. The latter were constructed using existing geological maps (Dreyfuss and Kuntz, 1969, 1970; Bonte, 1975; Chauve et al., 1979, 1983), complemented by our own field measurements, as well as by the available seismic and well data.

The Ognon Graben parallels the present-day valley of the Ognon River NNE of the La Serre Horst Structure and represents a small Paleogene depocenter as is evident from the occurrence of Oligocene synrift sediments (Chauve et al., 1983; Figs. 3, 5c and 4a). It strikes ENE–WSW and merges with the northern end of the Bresse Graben further to the west (Fig. 14b). In map view the location of the southern border fault of the Ognon Graben can only be traced in the north-eastern-most part of the study area, where it is delimited by the NE–SW striking Ognon Fault (OGF in Figs. 1 and 5). Along this fault, remnants of Oligocene rift sediments are also reported (Dreyfuss and Théobald, 1972). The OGF can be traced further to the north into the Vosges Mountains (Figs. 1 and 2), where it follows a major Paleozoic

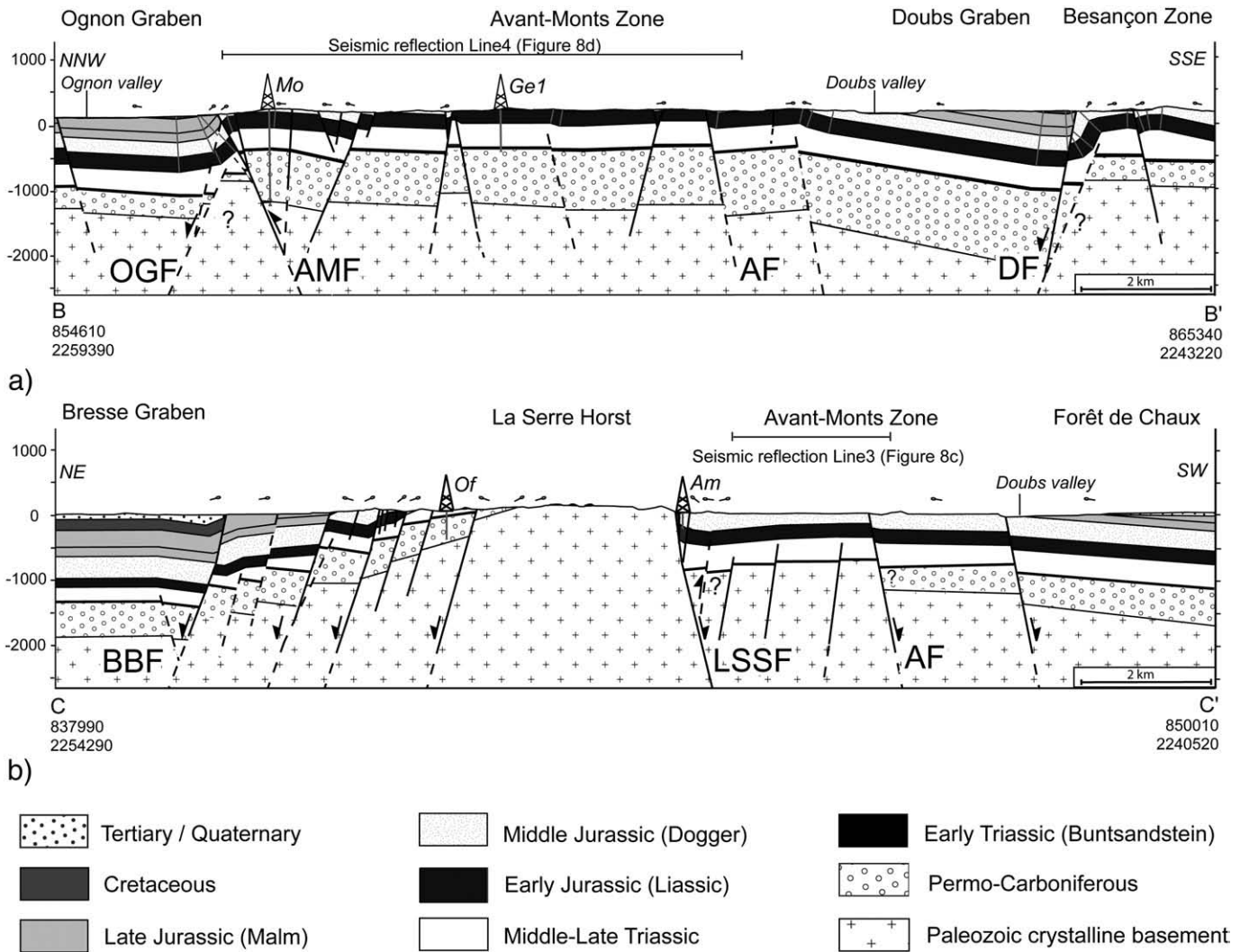


Fig. 14. Interpretative geological cross sections. See Figs. 3 and 5a–c for the location of cross sections wells and seismic reflection lines. AF: Arne Fault; AMF: Avant-Monts Fault; BBF: Bresse Border Fault; DF: Doubs Fault; LSSF: La Serre Southern Fault; OGF: Ognon Fault. a) Cross section across the Avant-Monts Zone. b) Cross section across the La Serre Horst.

lineament (Ruhland, 1959). This indicates that the Ognon Normal Fault, as a Cenozoic-age normal fault, probably reactivates a Paleozoic basement fault. South-westward we hypothesize that both faults bend and run further west along the ENE–WSW oriented Ognon Valley (Figs. 5 and 14a). Near its western termination the OGF delimits the La Serre Horst and then merges with the eastern Bresse Graben Border Fault (BBF in Figs. 1, 3, 5 and 14a–b).

The Avant-Monts Fault (AMF in Figs. 1, 3, 5 and 14a) represents a steep south-dipping reverse fault, as is shown from the seismic reflection data (Fig. 7d). The base Mesozoic subsurface map reveals that the Avant-Monts Fault forms the northern boundary of an ENE striking graben (Fig. 5a). These observations suggest that this reverse fault developed by inversion of a pre-existing normal fault and its presumed Late Paleozoic precursor, similar to the OGF.

The Arne Normal Fault (AF in Figs. 5, 7b–d, and 14a–b) strikes ENE–WSW and is interpreted as the southern boundary of the Paleozoic La Serre Horst Structure. Hence it also represents a Paleozoic fault that was reactivated in extensional mode (Figs. 7b–d and 14b). Together with the southerly adjacent Doubs Normal Fault (DF in Figs. 3, 5 and 14a) it forms the small ENE–WSW striking Doubs Graben that merges with the main Bresse Graben in the area of the Forêt de Chauv (Figs. 5a, and 14a,b). The Doubs Fault also marks the front of the thin-skinned Jura fold-and-thrust belt. Further to the east it is overridden by the thrust sheets of the Besançon Zone which is part of the Jura-fold-and-thrust

belt (Figs. 1, 3) and thus cannot be traced towards the southern Upper Rhine Graben (Madritsch et al., 2008).

Like the Ognon Fault, the Arne Fault and the Doubs Fault are marked by extensional flexures in the Mesozoic cover (Figs. 7b–d and 14a). Remnants of Cretaceous sediments are preserved in the flexure along the Doubs Fault (Chauve et al., 1979; Figs. 3, 5c and 14a) suggesting a post-Cretaceous age for flexure formation. The formation age of the flexures observed along the Arne Normal fault and other normal faults, depicted in the seismic reflection lines and geological cross sections (Figs. 7 and 14), are even less well defined due to the lack of sedimentary constrains. The initiation of flexuring as early as during Middle to Late Mesozoic extension (Wetzel et al., 2003) cannot be excluded. However, since the main depocenters observed in the area are of post-Mesozoic age, Cenozoic flexure formation seems by far more likely.

Based on these observations and interpretations we conclude that the La Serre Horst, first formed during the Late Paleozoic, was subsequently reactivated during Early Cenozoic extension forming a structural high between two Paleogene grabens (the Ognon and Doubs grabens, Fig. 14a). These grabens are bounded by ENE–WSE striking normal faults that caused extensional flexures within the Mesozoic cover (Fig. 14a), similar to those reported from the southern Upper Rhine Graben (Ustaszewski et al., 2005a; Ford et al., 2007). These ENE–WSW striking normal faults follow the orientation of the

Late Paleozoic Burgundy Trough System and are highly oblique to the faults bordering the Upper Rhine and Bresse grabens. This reveals their inherited character (Fig. 2). Most importantly, the inferred extension direction perpendicular to the strike of these normal faults, i.e. in a NW–SE direction, is in agreement with the paleostress data (stress tensor C; Fig. 10d).

7.3. Kinematics of Cenozoic deformation

The kinematic evolution of the RBTZ is inferred from the results of our paleostress analysis. The calculated paleostress tensor A, implying NNE–SSW-directed compression (Fig. 10b), is most probably related to the earliest post-Jurassic deformation phase that is recorded throughout the entire European platform (Bergerat, 1987; Dèzes et al., 2004). Most of the previous authors relate this compression to the Early Eocene Pyrenean orogeny (Bergerat, 1987; Lacombe et al., 1993; Rocher et al., 2003). Michon and Merle (2005), suggested that this phase is related to a Latest Cretaceous to Early Paleocene intra-plate compression, evidenced by the development of a regional erosional unconformity throughout the north-western Alpine foreland (Ziegler, 1990). Presumably, Eo-Oligocene rifting also initiated under a similar oriented stress field (Dèzes et al., 2004).

The strike-slip faults related to paleostress tensor A are overprinted by normal faults that define the paleostress tensors B and C indicating NE–SW and NW–SE extension, respectively. Similar extension directions are reported from regions adjacent to the study area but were variably interpreted. While some authors attribute them to individual regional paleostress fields of Late Mesozoic (Lacombe et al., 1990; Homberg et al., 2002) or Latest Oligocene age (Coulon and Frizon De Lamotte, 1988), Ustaszewski et al. (2005a) inferred that such different extension directions are the result of local stress and strain field perturbations that occur under one and the same general Eocene–Oligocene stress field.

Within our study area, NE–SW extension defined by paleostress tensor B is recorded exclusively around the La Serre Horst (Fig. 10c). Moreover, deciphering a reliable relative chronology between faults defining paleostress tensors B and C (Fig. 10d) based on crosscutting observations was not possible. Therefore we favour the idea that in our study area the paleostress tensor B reflects a local stress field perturbation rather than a separate stage of NE–SW directed extension. Similarly to what has been observed at the southern termination of the Upper Rhine Graben (Ustaszewski et al., 2005a) this perturbation could be the result of the interference between contemporaneous activity of ENE–WSW striking faults that dominate the RBTZ and N–S striking faults characteristic for the Bresse Graben and the grabens of the Massif Central (Merle et al., 1998).

Paleostress tensor C, indicating NW–SE extension (Fig. 10d), was by far more widely recognized and is thus interpreted as reflecting the main extensional event that led to the opening of the Upper Rhine and Bresse grabens in Late Eocene to Oligocene times. The observation that extension in the Rhine–Bresse Transfer Zone (RBTZ) is predominantly NW–SE orientated is in agreement with previous studies on brittle deformation that applied Direct Inversion paleostress methods (Bergerat, 1987; Lacombe et al., 1993).

In the area of the La Serre Horst the proposed coexistence of local NE–SW and the widely recognized NW–SE extension (tensors B and C in Fig. 10) locally results in a tectonic regime approaching radial extension (Fig. 15). This regime is characterized by well-clustered sub-vertical P-axes, a great-circle distribution of T-axes and R-value close to zero (Fig. 15). The latter was calculated using Direct Inversion analysis (Angelier, 1990) of the composite data that also showed NW–SE striking σ_3 . Similar observations are reported from the eastern termination of the RBTZ, i.e. at its intersection with the URG (Ustaszewski et al., 2005a).

Strike-slip faults that define paleostress tensor D indicating NE–SW compression (Fig. 10e) clearly post-date the normal faults related to

Paleogene extension. Such a compressional event has also been reported from the Burgundy area (Lacombe et al., 1990) and the northern Bresse Graben (Rocher et al., 2003). Nevertheless, the existence of NE–SW compression in the northern parts of the European Cenozoic Rift System (e.g. the southern URG) is controversial. While it was described by Bergerat (1987) as representing a regional Aquitanian stress field related to the build-up of collision-related stresses in the northern Alpine foreland it was not detected by Lopes-Cardozo and Behrmann (2006). Sub-surface investigations along the URG (Rotstein et al., 2005a) and analogue modelling studies of this part of the rift system (Michon and Sokoutis, 2005) also speak against the existence of a regional NE–SW compressional stress field. During our investigation this paleostress tensor D was detected only locally, mainly at the south-eastern termination of the RBTZ, near the La Serre Horst. Similarly to what was observed in the adjacent northern Bresse Graben area (Rocher et al., 2003), this stress tensor is rather the consequence of a permutation between σ_2 and σ_1 during the extensional event defined by paleostress tensor C (Figs. 9 and 10d–e) while the orientation of σ_3 remains approximately constant. Hence, paleostress tensor D may also reflect local stress field perturbations in the RBTZ during the latest stage of rifting rather than an individual regional paleostress field.

Paleostress tensor E indicating roughly NW–SE compression is very well constrained throughout the entire area of investigation (Fig. 10f). It is interpreted to reflect the youngest deformation event related to Late Miocene to recent Alpine collision processes. This deformation propagated far northward into the distal foreland of the Alps (Rocher et al., 2004). At first, shortening was restricted to the Mesozoic cover, when the formation of the thin-skinned Jura fold-and-thrust belt started and when the north-westernmost segment of the decoupled cover (the Besançon Zone) encroached onto the RBTZ (Madritsch et al., 2008). However from the Early Pliocene onwards, this compression also affected the underlying crystalline basement and induced thick-skinned reactivation of pre-existing basement faults related to the formation of the RBTZ in particular and the southern Upper Rhine Graben in general (Giamboni et al., 2004; Rotstein et al., 2005b; Ustaszewski and Schmid, 2007). In our study area this style of deformation is manifested by the steeply dipping Avant-Monts reverse fault. The reverse movement along this fault was probably accompanied by the reactivation of the La Serre Southern Fault and the Ognon Normal Fault, leading to partial inversion of the RBTZ in a dextral transpressional regime (Madritsch et al., 2008).

In summary, the complex fracture inventory detected throughout the RBTZ (Fig. 10) is interpreted to be related to 3 major deformation stages: i) Post Jurassic NNE–SSW shortening probably related to the Pyrenean orogeny ii) NW–SE extension related to formation of the

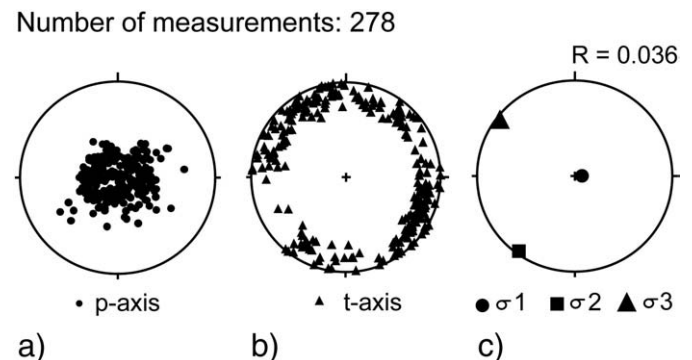


Fig. 15. Extension directions from 11 sites around the La Serre Horst where paleostress tensors B and C were reconstructed (compare Figs. 9 and 10 and Table 2). Superposition of both tensors results in a local tectonic regime approaching radial extension. a) Composite p-axes plot. b) Composite t-axes plot. c) Direct Inversion of the composite data set yielding overall NW–SE orientation of the minimum principal stress axis (σ_1) and R-value close to zero indicating radial extension. All plots are equal in area, lower hemisphere projections. $R = (\sigma_2 - \sigma_3) / (\sigma_1 - \sigma_3)$.

ECRIS. Locally, the strain and stress pattern shows perturbations due to the reactivation of ENE–WSW striking pre-existing structures. During the latest stages of rifting permutation between σ_1 and σ_2 resulted in local strike-slip faulting. iii) NW–SE shortening related to Alpine collision.

7.4. Strike-slip dominated transform zone or oblique graben?

Finally we discuss our combined dataset in the light of the tectonic concepts regarding the formation of the RBTZ. Two distinct kinematic models for its formation were proposed (Fig. 16). A first one, by Contini and Theobald (1974) and Bergerat (1977) suggested that E–W extension in the Rhine and Bresse grabens occurred under a dominant N–S compression and was transferred along the RBTZ by pure strike-slip reactivation of a pre-existing basement fault (Fig. 16a). Lacombe et al. (1993) modified this concept and suggested that the RBTZ formed by sinistrally transtensional reactivation of such ENE–WSW striking basement fault systems under overall E–W extension (Fig. 16b). Thereby the NW–SE extension that was recorded within the RBTZ is regarded as reflecting local stress (and strain) perturbations within the sedimentary cover under crustal-scale E–W directed extension during the formation of the European Cenozoic Rift System. Furthermore, these authors suggest that large-scale and deep-seated wrench faulting, reactivating the pre-existing Paleozoic ENE–WSW striking fault system, could cause such perturbations at shallow depth. More recently, ENE–WSW to NW–SE extension directions were also inferred for the Upper Rhine Graben (Michon and Sokoutis, 2005; Hinsken et al., 2007). Thus, it seems perfectly feasible that this extension direction simply results from extensional reactivation of the pre-existing Burgundy Trough System.

In any case, our data do not support the idea that the RBTZ represents a distinct intra-continental transform zone dominated by strike-slip tectonics (Fig. 16a). Instead, following Hinsken et al. (2007), we propose that the RBTZ represents an inherited and oblique graben segment within the European Cenozoic Rift System, which is by its own also dominated by extension rather than by strike-slip or wrench faulting (Fig. 16c). We share this conclusion based on the following lines of evidence:

- 1) The apatite fission track analyses show that the Late Paleozoic La Serre Horst experienced significant amount of exhumation during the Eo-Oligocene formation of the RBTZ (Figs. 11 and 13). This requires a substantial extension and pleads against a pure strike-slip mode of deformation within the RBTZ.
- 2) Subsurface data document that basement reactivation was mainly extensional and led to the formation of major ENE–WSW striking normal faults, the most notable examples being the Ognon, Avant-Monts, Arne and Doubs faults. These faults are parallel to the ENE–WSW aligned Paleogene graben and horst structures that are oriented highly oblique to the overall trend of the European Cenozoic Rift System. The fact that these faults are also parallel to the Late Paleozoic Burgundy Trough and the La Serre Horst emphasizes their inherited nature. Existence of distinctive flexures associated with most of these faults suggests a predominantly extensional rather than strike-slip character of the reactivation (Figs. 8 and 14 a–b).
- 3) Individual major ENE–WSW striking normal faults that are part of the fault set characterizing the Rhine–Bresse Transfer Zone cannot be directly interconnected to each other across the area between the Upper Rhine and the Bresse grabens. The Ognon Fault that inherited from a Paleozoic normal fault, for example, cannot be traced into the southern Upper Rhine Graben itself, but rather bends to the NNE and runs into the Vosges Mountains (Ruhland, 1959). Hence, the Ognon Normal Fault is not capable to transfer extension from the Bresse Graben to the southern Upper Rhine Graben by pure sinistral strike-slip or sinistrally transtensional

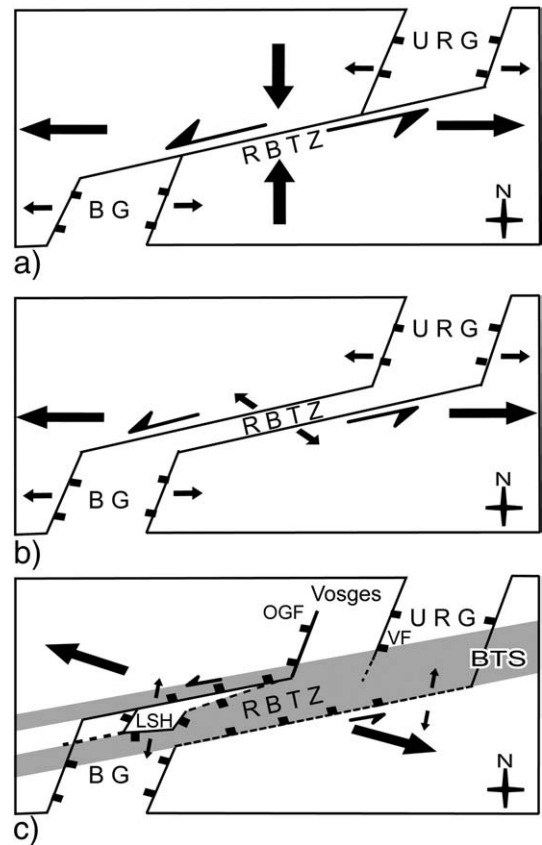


Fig. 16. Comparison of genetic and kinematic models for the formation of the Rhine–Bresse Transfer Zone: a) N–S compression resulting in E–W extension along the Rhine and Bresse graben and formation of the RBTZ by pure strike-slip reactivation of a pre-existing basement fault (Contini and Theobald, 1974; Bergerat, 1977). b) Overall E–W extension causes sinistral transtensional reactivation of a basement fault that leads to stress perturbations with σ_3 trending NW–SE in the RBTZ (Lacombe et al., 1993). c) Overall NW–SE extension leads to the oblique extensional reactivation of the Burgundy Trough and La Serre Horst with a minor sinistral transtensional strike-slip component (this study). Reactivation of the pre-existing horst results in local stress field perturbation characterised by variable extension directions. BG: Bresse graben; BTS: Burgundy Trough System; LSH: La Serre Horst; OGF: Ognon Fault; RBTZ: Rhine–Bresse Transfer Zone; URG: Upper Rhine Graben; Vf: Vosges Fault.

movement. This is further supported by the observations of Ford et al. (2007), who found that the western border fault of the Upper Rhine Graben (Vosges Fault), which represents the most likely candidate to form the eastern connection of the Ognon Fault, does not connect into the RBTZ but rather dies out east to the city of Montbéliard (Figs. 1 and 2).

- 4) At the outcrop scale dip-slip normal faults are dominant throughout the area. The paleostress tensor C calculated by the Right-Dihedra method indicates that extension is oriented slightly oblique to the NW–SE striking structural grain of the RBTZ. Locally the stress and strain fields are perturbed due to the extensional reactivation of pre-existing structures like the La Serre Horst Structure.

8. Conclusions

The combined results of surface and subsurface structural analyses, paleostress determinations and thermochronological dating document multiple reactivation of Late Paleozoic basement structures throughout the area of the Rhine–Bresse Transfer Zone exerting a strong influence on Cenozoic fault geometries and kinematics.

The zircon fission track data from the La Serre Horst document a Middle Jurassic to Early Cretaceous heating event at temperatures that probably were not higher than 200–250 °C. Furthermore, the zircon FT

ages, combined with modelling of the apatite FT data, reveal two distinct periods of cooling. A first cooling event, probably related to thermal relaxation, occurred in the Early Cretaceous was followed by extremely slow cooling at a high geothermal gradient until the end of the Eocene. A second rapid cooling event begins at around 38 to 32 Ma and is interpreted to reflect substantial extensional reactivation of the La Serre Horst during Eocene–Oligocene rifting, i.e. the main stage of the RBTZ formation. In the area of the La Serre Horst this period was associated with substantial uplift and erosion. Neogene to present exhumation of the La Serre Horst is related to compression-induced uplift and erosion driven by the Alpine collision. This collision caused by lithospheric deformation induced Early to Middle Miocene differential uplift, and Early Pliocene to recent and probably largely thick-skinned shortening, once more reactivating the multiply pre-structured RBTZ.

Subsurface analysis confirms that the structural grain of the RBTZ is defined by the reactivation of Late Paleozoic basement structures. This reactivation resulted in the formation of two main sets of Cenozoic normal faults. A NNE–SSW striking normal fault set, oriented parallel to the Rhine and Bresse grabens and a second major normal ENE–WSW striking normal fault set inherited from the pre-existing Late Paleozoic Burgundy Trough System and the La Serre Horst Structure.

Paleostress analyses revealed a complex multi-stage deformation history of the study area. The stress and strain fields appear to be inhomogeneous and characterized by perturbations most likely caused by reactivation of pre-existing structures. During Eo-Oligocene formation of the RBTZ the dominant ENE–WSW striking fault set predominantly accommodated NW–SE extension rather than sinistral strike-slip motion.

On a larger scale the results of this study confirm the view that the RBTZ formed by structural inheritance of pre-existing Late Paleozoic basement structures. We suggest that Paleogene reactivation produced a separate oblique graben segment within the European Cenozoic Rift system in the form of the RBTZ, which hence does not represent a strike-slip dominated transform zone.

Acknowledgments

This project was funded by ELTEM and carried out within the framework of the EUCOR URGENT project. The authors are indebted to Gaz de France for the authorization to analyze and publish seismic reflection data. Furthermore the authors would like to thank H. Dresmann, S. Hinsken, O. Lacombe and P. A. Ziegler for discussions on the data and comments on earlier versions of the manuscript as well as the entire past and present EUCOR-URGENT team at the Geological Institute at Basel University. Careful reviews by L. Michon and M. Rocher, as well as additional comments by the journal editor, significantly improved the original manuscript.

Appendix A. Supplementary data

Supplementary data associated with this article can be found, in the online version, at doi:10.1016/j.tecto.2009.02.044.

References

- Angelier, J., 1989. From orientation to magnitudes in paleostress determinations using fault slip data. *Journal of Structural Geology* 11, 37–50.
- Angelier, J., 1990. Inversion of field data in fault tectonics to obtain the regional stress – III. A new rapid direct inversion method by analytical means. *Geophysical Journal International* 103, 363–376.
- Angelier, J., Mechler, P., 1977. Sur une méthode graphique de recherche des contraintes principales également utilisable en tectonique et en sismologie: la méthode des dièdres droits. *Bulletin de la Société Géologique de France* 19, 1309–1318.
- Barbarand, J., Lucazeau, F., Pagel, M., Sèrannée, O., 2001. Burial and exhumation history of the south eastern Massif Central (France) constrained by apatite fission-track thermochronology. *Tectonophysics* 335, 275–290.
- Berger, J.P., Reichenbacher, B., Becker, D., Grimm, M., Grimm, K., Picot, L., Storni, A., Pirkenseer, C., Derer, C., Schaefer, A., 2005. Paleogeography of the Upper Rhine Graben (URG) and the Swiss Molasse Basin (SMB) from Eocene to Pliocene. *International Journal of Earth Sciences* 94, 697–710.
- Bergerat, F., 1977. La fracturation de l'avant-pays jurassien entre les fossés de la Saône et du Rhin. Analyse et essai d'interprétation dynamique. *Revue de Géographie Physique et de Géologie Dynamique* 14, 325–338 (2).
- Bergerat, F., 1987. Stress fields in the European platform at the time of Africa–Eurasia collision. *Tectonics* 6, 99–132.
- Bergerat, F., Chorowicz, J., 1981. Etude des images Landsat de la zone transformante Rhin–Saône (France). *Geologische Rundschau* 70, 354–367.
- Bergerat, F., Mugnier, J.L., Guellec, S., Truffert, C., Cazes, M., Damotte, B., Roure, F., 1990. Extensional tectonics and subsidence of the Bresse basin. An interpretation from ECORS data. In: Roure, F., Heitzmann, P., Polino, R. (Eds.), *Deep Structure of the Alps 1*. Soc. Geol. It. Zürich. *Mémoire de la Société géologique de la Suisse*, pp. 145–156. vol. spec.
- Boigk, H., Schönreich, H., 1970. Die Tiefenlagen der Permabasis im nördlichen Teil des Oberrheingrabens. In: Illies, J.H., Mueller, S. (Eds.), *Graben Problems*. Proceedings of an International Rift Symposium held in Karlsruhe 1968, International Upper Mantle Project. E. Schweitzerbart, Stuttgart'sche, pp. 45–55.
- Bonte, A., 1975. Carte géol. France (1/50000), feuille Quingey, XXXIII-24. BRGM.
- Bourgeois, O., Ford, M., Diraison, C., Le Carlier de Veslud, M., Gerbault, R., Pik, N., 2007. Separation of rifting and lithospheric folding signatures in the NW-Alpine foreland. *International Journal of Earth Sciences*, 96, 1003–1031.
- Burkhard, M., 1990. Aspects of the large-scale Miocene deformation in the most external part of the Swiss Alps (Subalpine Molasse to Jura fold belt). *Eclogae Geologicae Helveticae* 83, 559–583.
- Brandon, M.T., Roden-Tice, M.K., Garver, J.I., 1998. Late Cenozoic exhumation of the Cascadia accretionary wedge in the Olympic Mountains, northwest Washington State. *GSA Bulletin* 110, 985–1009.
- Brockamp, O., Zuther, M., 1983. Das Uranvorkommen Müllenbach/Baden-Baden, eine epigenetisch-hydrothermale Imragnationslagerstätte in Sedimenten des Oberkarbon, Teil II. Das Nebengestein. *N. Jahrb. Mineral. Abh.* 148, 22–33.
- Burtner, L.R., Nigrini, A., Donelik, R.A., 1994. Thermochronology of Lower Cretaceous source rocks in the Idaho–Wyoming thrust belt. *AAPG Bulletin* 78, 1613–1636.
- Carlson, D.W., Donelick, R.A., Ketchum, R.A., 1999. Variability of apatite fission-track annealing kinetics. I. Experimental results. *American Mineralogist* 84, 1213–1223.
- Chauve, P., Kerrien, Y., Pernin, C., 1979. Carte géol. France (1/50000), feuille Dole XXXII-24. BRGM.
- Chauve, P., Enay, R., Fluck, P., Sittler, C., 1980. L'Est de la France (Vosges, Fossé Rhénan, Bresse, Jura). *Annales scientifiques de l'Université de Besançon* 4, 3–80.
- Chauve, P., Campy, M., Pernin, C., Morre-Biot, N., 1983. Carte géol. France (1/50000), feuille Pesmes, XXXII-23. BRGM.
- Choulet, F., Faure, M., Fabbri, O., 2007. The Autun Shear zone: age, kinematics, significance and regional correlations. Mechanism of Variscan Orogeny: A Modern View on Orogenic Research". Proceedings Special Meeting of the French and Czech Geological Societies, vol. 2. *Géologie de la France*, p. 82.
- Contini, D., Theobald, N., 1974. Relations entre le fossé rhénan et le fossé de la Saône. *Tectonique des régions sous-vosgiennes et préjurassiennes*. In: Illies, J.H., Fuchs, K. (Eds.), *Approaches to Taphrogenesis*. Sci. Rep., vol. 8, pp. 309–321.
- Coromina, G., Fabbri, O., 2004. Late Palaeozoic NE–SW ductile–brittle extension in the La Serre Horst, eastern France. *Comptes Rendus Geosciences* 336, 75–84.
- Corrigan, J.D., 1993. Apatite fission-track analysis of Oligocene strata in South Texas, USA: testing annealing models. *Chemical Geology* 104, 227–249.
- Coulon, M., Frizon de Lamotte, D., 1988. Les extensions cénozoïques dans l'Est du bassin de Paris. *Comptes Rendus de l'Académie des Sciences Paris* 307, 1111–1119.
- Debrand-Passard, S., Courbouleix, S., 1984. Synthèse Géologique du Sud-Est de la France, volume 2. Atlas comprenant 64 planches en couleurs, *Mémoire du Bureau de recherches géologiques et minières*, vol. 126. BRGM, p. 614.
- Dèzes, P., Schmid, S.M., Ziegler, P.A., 2004. Evolution of the European Cenozoic Rift System. interaction of the Alpine and Pyrenean orogens with their foreland lithosphere. *Tectonophysics* 389, 1–33.
- Diebold, P., Naef, H., 1990. Der Nordschweizer Permkarbonatrog. *Nagra informiert* 2, 29–36.
- Dreyfuss, M., Kuntz, G., 1969. Carte géol. France (1/50000), feuille Besançon, XXXII-23. BRGM.
- Dreyfuss, M., Kuntz, G., 1970. Carte géol. France (1/50000), feuille Gy, XXXIII-22. BRGM.
- Dreyfuss, M., Théobald, N., 1972. Carte géol. France (1/50000), feuille Baume-les-Dames, XXXIV-22. BRGM.
- Dumitru, T.A., 1995. A new computer automated microscope stage system for fission track analysis. *Nuclear Tracks Radiation Measurements* 21, 575–580.
- Echtler, H., Malavielle, J., 1990. Extensional basement uplift and Stephano-Permian collapse basin in a Late Variscan metamorphic core complex (Montagne Noire, Southern Massif Central). *Tectonophysics* 177, 125–138.
- Echtler, H.P., Chauvet, A., 1991–1992. Carboniferous convergence and subsequent crustal extension in the southern Schwarzwald (SW Germany). *Geodinamica Acta* 5, 37–49.
- Eisbacher, G., Lüschen, E., Wickert, F., 1989. Crustal scale thrusting and extension in the Hercynian Schwarzwald and Vosges, Central Europe. *Tectonics* 8, 1–21.
- Elmohandes, S.-E., 1981. The Central European Graben System. Rifting imitated by clay modelling. *Tectonophysics* 73, 69–78.
- Fleury, R., Farjanel, G., Collin, J.-J., 1982. Carte géol. France (1/50000), feuille Saurer, XXXI-24. BRGM.
- Ford, M., Le Carlier de Veslud, C., Bourgeois, O., 2007. Kinematic and geometric analysis of fault related folds in a rift setting. The Danne-Marie basin, Upper Rhine Graben, France. *Journal of Structural Geology* 29, 1811–1830.
- Galbraith, R.F., Laslett, G.M., 1993. Statistical models for mixed fission-track ages. *Nuclear Tracks and Radiation Measurements* 21, 459–470.

- Gallagher, K., 1995. Evolving temperature histories from apatite fission-track data. *Earth and Planetary Sciences Letters* 136, 421–435.
- Giamboni, M., Ustaszewski, K., Schmid, S.M., Schumacher, M.E., Wetzel, A., 2004. Pliocene transpressional reactivation of Paleozoic and Paleogene structures in the Rhine–Bresse Transform Zone (northern Switzerland and eastern France). *International Journal of Earth Sciences* 93, 207–223. doi:10.1007/s00531-003-0375-2.
- Gleadow, A.J.W., Duddy, I.R., Green, P.F., Hegarty, K.A., 1986. Fission track length in the apatite annealing zone and interpretation of mixed ages. *Earth and Planetary Science Letters* 78, 245–254.
- Green, P.F., 1981. A new look at statistics in fission track dating. *Nuclear Tracks and Radiation Measurements* 5, 77–86.
- Green, P.F., Duddy, I.R., 1989. Some comments on paleotemperature estimation from apatite fission track analysis. *Journal of Petroleum Geology* 12, 111–114.
- Green, P.F., Duddy, I.R., Gleadow, A.J.W., Tingate, P.R., 1985. Fission-track annealing in apatite, track length measurements and the form of the Arrhenius plot. *Nuclear Tracks and Radiation Measurements* 10, 323–328.
- Green, P.F., Duddy, I.R., Gleadow, A.J.W., Tingate, P.R., Laslett, G.M., 1986. Thermal annealing of fission tracks in apatite, 1. A qualitative description. *Chemical Geology* 59, 237–253.
- Hinsken, S., Ustaszewski, K., Wetzel, A., 2007. Graben width controlling syn-rift sedimentation: the Palaeogene southern Upper Rhine Graben as an example. *International Journal of Earth Sciences* 96, 979–1002.
- Homberg, C., Bergerat, F., Philippe, Y., Lacombe, O., Angelier, J., 2002. Structural inheritance and Cenozoic stress fields in the Jura fold-and-thrust belt (France). *Tectonophysics* 357, 137–158.
- Hurford, A.J., Green, P.F., 1983. The zeta age calibration of fission-track dating. *Chemical Geology* 41, 285–317.
- Illies, J.H., 1972. The Rhinegraben rift system – plate tectonics and transform faulting. *Geophysical Surveys* 1, 27–60.
- Illies, J.H., 1981. Mechanism of graben formation. *Tectonophysics* 73, 249–266.
- Jowett, E.C., 1991. Post-collisional formation of the Alpine foreland rifts. *Annales Geological Society of Poland* 61, 37–59.
- Lacombe, O., Angelier, J., Laurent, P., Bergerat, F., Tournet, C., 1990. Joint analyses of calcite twins and fault slips as a key for deciphering polyphase tectonics. Burgundy as a case study. *Tectonophysics* 182, 279–300.
- Lacombe, O., Angelier, J., Byrne, D., Dupin, J., 1993. Eocene–Oligocene tectonics and kinematics of the Rhine–Saône continental transform zone (eastern France). *Tectonics* 12, 874–888.
- Lancelot, J., Briquieu, L., Respaut, J.P., Clauer, N., 1995. Géochimie isotopique des systèmes U–Pb/Pb–Pb et évolution polyphasée des gîtes d'uranium du Lodévois et du sud du Massif Central. *Chronique de la Recherche minière* 521, 3–18.
- Larroque, J., Laurent, P., 1988. Evolution of the stress field pattern in the south of the Rhine Graben from the Eocene to the present. *Tectonophysics* 148, 41–58.
- Laslett, G.M., Green, P.F., Duddy, I.R., Gleadow, A.J.W., 1987. Thermal annealing of fission tracks in apatite 2. A Quantitative Analysis. *Chemical Geology* 65, 1–13.
- Laubscher, H., 1970. Grundsätzliches zur Tektonik des Rheingrabens. In: Illies, J.H., Mueller, S. (Eds.), *Graben Problems. Proceedings of an International Rift Symposium held in Karlsruhe 1968, International Upper Mantle Project. E. Schweizerbart'sche, Stuttgart*, pp. 79–86.
- Laubscher, H., 1972. Some overall aspects of Jura dynamics. *American Journal of Science* 272, 293–304.
- Laubscher, H., 1992. Jura kinematics and the Molasse Basin. *Eclogae Geologicae Helveticae* 85, 653–675.
- Lopes-Cardozo, G.G.O., Behrmann, J.H., 2006. Kinematic analysis of the Upper Rhine Graben boundary fault system. *Journal of Structural Geology* 28, 1028–1039.
- Macquar, J.-C., 1984. Minéralisation triasiques en Pb, Zn, Ba (Cu, Fe) du Bassin subalpin. typologie, chronologie, contrôles et modèles. In: Debrand-Passard, S., Courbouleix, S.M.J., L. (Eds.), *Synthèse géologique du Sud-Est de la France- stratigraphie et paléogéographie*, vol. 125. *Mém. Bur. Rech. Géol. Min.*, pp. 112–118.
- Madritsch, H., 2008. Structural evolution and neotectonics of the Rhine–Bresse Transfer Zone (eastern France). Unpublished PhD-Thesis, Universität Basel, 178 pp.
- Madritsch, H., Schmid, S.M., Fabbri, O., 2008. Interactions between thin- and thick-skinned tectonics at the northwestern front of the Jura fold-and-thrust-belt (eastern France). *Tectonics* 27, TC5005. doi:10.1029/2008/TC002282.
- Marrett, R., Allmendinger, R.W., 1990. Kinematic analysis of fault-slip data. *Journal of Structural Geology* 12, 973–986.
- Marrett, R., Peacock, D.C.P., 1999. Strain and stress. *Journal of Structural Geology* 21, 1057–1063.
- McCann, T., Pascal, C., Timmerman, M.J., Krzywiec, P., López-Gómez, J., Wetzel, A., Krawczyk, C.M., Rieke, H., Lamarque, J., 2006. Post-Variscan (end Carboniferous–Early Permian) basin evolution in Western and Central Europe. In: Gee, D.G., Stephenson, R.A. (Eds.), *European Lithosphere Dynamics*, vol. 32. *Geological Society of London Memoirs*, pp. 355–388.
- Merle, O., Michon, L., 2001. The formation of the West European rift: a new model as exemplified by the Massif Central area. *Bulletin de la Société de Géologie de France* 172, 213–221.
- Merle, O., Michon, L., Camus, G., de Goer, A., 1998. L'extension oligocène sur la transversale septentrionale du rift du Massif Central. *Bulletin de la Société de Géologie de France* 109, 615–626.
- Meschede, M., Decker, K., 1993. Störungsflächenanalyse entlang des Nordrandes der Ostalpen – ein methodischer Vergleich. *Zeitschrift der Deutschen Geologischen Gesellschaft* 144, 419–433.
- Michon, L., Merle, O., 2001. The evolution of the Massif Central Rift: spatio-temporal distribution of the volcanism. *Bulletin de la Société de Géologie de France* 172, 69–80.
- Michon, L., Merle, O., 2005. Discussion on "Evolution of the European Cenozoic Rift System: interaction of the Alpine and Pyrenean orogens with their foreland lithosphere by P. Dèzes, S.M. Schmid, P.A. Ziegler, *Tectonophysics* 389 (2004) 1–33. *Tectonophysics* 401, 251–256.
- Michon, L., Sokoutis, D., 2005. Interaction between structural inheritance and extension direction during graben formation: an experimental approach. *Tectonophysics* 409, 125–146.
- Morre, N., Thiébaud, J., 1961. Etude pétrographique des roches cristallines découvertes par sondage profonds entre Vosges et Morvan. *Extrait des Annales scientifiques de l'Université de Besançon* 14, 73–83.
- Neugebauer, H.J., 1978. Crustal doming and mechanism of rifting: Part 1, rift formation. *Tectonophysics* 45, 159–186.
- O'Sullivan, P., Parrish, R., 1995. The importance of apatite composition and single-grain ages when interpreting fission track data from plutonic rocks: a case study from the Coast ranges, British Columbia. *Earth and Planetary Science Letters* 132, 213–224.
- Petit, J.P., 1987. Criteria for the sense of movement on fault surfaces in brittle rocks. *Journal of Structural Geology* 9, 597–608.
- Pfiffner, O.A., Burkhard, M., 1987. Determination of paleo-stress axes orientations from fault, twin and earthquake data. *Annales Tectonicae* 1, 48–57.
- Rat, P., 1976. Structures et phases de structuration dans les plateaux bourguignons et le Nord Ouest du fossé bressan (France). *Geologische Rundschau* 65, 101–126.
- Reiter, F., Acs, P., 1996–2000. *TectonicsFP. Computer Software for Structural Geology, Version 2.0 PR.* <http://www.tectonicsfp.com/>.
- Rey, P., Burg, J.-P., Caron, J.-M., 1991–1992. Middle and Late Carboniferous extension in the Variscan Belt: structural and petrological evidences from the Vosges massif (eastern France). *Geodinamica Acta* 5, 17–36.
- Rocher, M., Chevalier, F., Petit, C., Guiraud, M., 2003. Tectonics of the Northern Bresse region (France) during the Alpine cycle. *Geodinamica Acta* 16, 131–147.
- Rocher, M., Cushing, M., Leimeille, F., Lozach, Y., Angelier, J., 2004. Intraplate paleostresses reconstructed with calcite twinning and faulting: improved method and application to the eastern Paris Basin (Lorraine, France). *Tectonophysics* 387, 1–21.
- Rotstein, Y., Behrmann, J.H., Lutz, M., Wirsing, G., Luz, A., 2005a. Tectonic implications of transpression and transtension. *Tectonics* 24, TC6001. doi:10.1029/2005TC001797.
- Rotstein, Y., Schaming, M., Rouse, S., 2005b. Structure and tertiary tectonic history of the Mulhouse High, Upper Rhine Graben: block faulting modified by changes in the Alpine stress regime. *Tectonics* 24, TC1012. doi:10.1029/2004TC001654.
- Roure, F., 2008. Foreland and hinterland basins: what controls their evolution? *Swiss Journal of Geosciences* 101 (Supplement 1), S5–S29.
- Ruhland, M., 1959. Une dislocation majeure du socle Vosgien dans la haute Vallée de l'Ognon. *Bulletin du Service de la carte géologique d'Alsace et de Lorraine* 12, 61–64.
- Schmid, S.M., Pfiffner, O.A., Fritzsche, N., Schönborn, G., Kissling, E., 1996. Geophysical–geological transect and tectonic evolution of the Swiss–Italian Alps. *Tectonics* 15, 1036–1064.
- Schumacher, M.E., 2002. Upper Rhine Graben: role of preexisting structures during rift evolution. *Tectonics* 21 (1), 6–16–17.
- Sengör, A.M.C., 1976. Collision of irregular continental margins: implications for foreland deformation of Alpine-type orogens. *Geology* 4, 779–782.
- Séranne, M., 1999. The Gulf of Lion continental margin (NW Mediterranean) revisited by IBS: an overview. In: Durand, B., Jolivet, L., Horvath, F., Séranne, M. (Eds.), *The Mediterranean Basins: Tertiary Extension within the Alpine Orogen. Spec. Publ.*, vol. 156. *Geol. Soc. London*, pp. 15–36.
- Seward, D., 1989. Cenozoic basin histories determined by fission track dating of basement granites, South Island, New Zealand. *Chemical Geology* 79, 31–48.
- Sissingh, W., 1998. Comparative tertiary stratigraphy of the Rhine Graben, Bresse Graben and Molasse Basin: correlation of Alpine foreland events. *Tectonophysics* 300, 249–284.
- Surma, F., Geraud, Y., Pourcelot, L., Gauthier-Lafaye, F., Clavaud, J.B., Zamora, M., Lespinasse, M., Cathelineau, M., 2003. Microstructures d'un grès affecté par une faille normale; anisotropie de connectivité et de perméabilité. *Bulletin de la Société Géologique de France* 174, 295–303.
- Tagami, T., 2005. Zircon fission-track thermochronology and applications to fault studies. *Reviews in Mineralogy and Geochemistry* 58 (1), 95–122.
- Tagami, T., Shimada, C., 1996. Natural long-term annealing of the zircon fission track system around a granitic pluton. *Journal of Geophysical Research* 101, 8245–8255.
- Tagami, T., Galbraith, R.F., Yamada, R., Laslett, G.M., 1998. Revised annealing kinetics of fission tracks in zircon and geological implications. In: Van den Haute, P., de Corte, F. (Eds.), *Advances in Fission-track Geochronology. Solid Earth Sci. Libr.*, vol. 10. *Kluwer Acad., Norwell, Mass.*, pp. 99–112.
- Timar-Geng, Z., Fügenschuh, B., Schaltegger, U., Wetzel, A., 2004. The impact of the Jurassic hydrothermal activity on zircon fission track data from the southern Upper Rhine Graben area. *Schweizerische Mineralogische und Petrographische Mitteilungen* 84, 257–269.
- Timar-Geng, Z., Fügenschuh, B., Wetzel, A., Dresmann, H., 2006. Low-temperature thermo-chronology of the flanks of the southern Upper Rhine Graben. *International Journal of Earth Sciences* 95, 685–702.
- Ustaszewski, K., Schmid, S.M., 2007. Latest Pliocene to recent thick-skinned tectonics at the Upper Rhine Graben – Jura Mountains junction. *Swiss Journal of Geosciences* 100, 293–312.
- Ustaszewski, K., Schumacher, M.E., Schmid, S.M., 2005a. Simultaneous normal faulting and extensional flexuring during rifting – an example from the southernmost Upper Rhine Graben. *International Journal of Earth Sciences* 94, 680–696.
- Ustaszewski, K., Schumacher, M.E., Schmid, S.M., Nieuwland, D., 2005b. Fault reactivation in brittle-viscous wrench systems – dynamically scaled analogue models and application to the Rhine–Bresse Transfer Zone. *Quaternary Science Reviews* 24, 363–380.
- Wallace, R.E., 1951. Geometry of shearing stress and relation to faulting. *Journal of Geology* 59, 118–130.

- Wetzel, A., Allenbach, R., Allia, V., 2003. Reactivated basement structures affecting the sedimentary facies in a tectonically “quiescent” epicontinental Basin: an example from NW Switzerland. *Sedimentary Geology* 157, 153–172.
- Yamada, R., Tagami, T., Nishimura, S., Ito, H., 1995. Annealing kinetics of fission tracks in zircon: an experimental study. *Chemical Geology* 122, 249–258.
- Ziegler, P., 1986. Geodynamic model for the Paleozoic crustal consolidation of Western and Central Europe. *Tectonophysics* 126, 303–328.
- Ziegler, P.A., 1990. Geological atlas of Western and Central Europe. Shell Internationale Petroleum Maatschappij B.V. Den Haag, pp. 1–238.
- Ziegler, P.A., 1992. European Cenozoic rift system. *Tectonophysics* 208, 91–111.
- Ziegler, P., Dèzes, P., 2007. Cenozoic uplift of Variscian Massifs in the foreland of the Alpine foreland: timing and controlling mechanisms. *Global and Planetary Change* 58, 237–269.
- Ziegler, P.A., Schumacher, M.E., Dèzes, P., van Wees, J.-D., Cloetingh, S., 2004. Post-Variscan evolution of the lithosphere in the Rhine Graben area: constraints from subsidence modelling. In: Wilson, M. (Ed.), *Permo-Carboniferous Magmatism and Rifting in Europe*. Geological Society of London Special Publications, vol. 223. Geological Society, pp. 289–317.